NASA Technical Memorandum 4769

Thermostructural Behavior of a Hypersonic Aircraft Sandwich Panel Subjected to Heating on One Side

William L. Ko

April 1997

NASA Technical Memorandum 4769

Thermostructural Behavior of a Hypersonic Aircraft Sandwich Panel Subjected to Heating on One Side

William L. Ko
Dryden Flight Research Center
Edwards, California

CONTENTS

TABLES

ABSTRACT

Thermostructural analysis was performed on a heated titanium honeycomb-core sandwich panel. The sandwich panel was supported at its four edges with spar-like substructures that acted as heat sinks, which are generally not considered in the classical analysis. One side of the panel was heated to high temperature to simulate aerodynamic heating during hypersonic flight. Two types of surface heating were considered: (1) flat-temperature profile, which ignores the effect of edge heat sinks, and (2) dome-shaped-temperature profile, which approximates the actual surface temperature distribution associated with the existence of edge heat sinks. The finite-element method was used to calculate the deformation field and thermal stress distributions in the face sheets and core of the sandwich panel. The detailed thermal stress distributions in the sandwich panel are presented, and critical stress regions are identified. The study shows how the magnitudes of those critical stresses and their locations change with different heating and edge conditions. This technical report presents comprehensive, three-dimensional graphical displays of thermal stress distributions in every part of a titanium honeycomb-core sandwich panel subjected to hypersonic heating on one side. The plots offer quick visualization of the structural response of the panel and are very useful for hot structures designers to identify the critical stress regions.

NOMENCLATURE

a	length of sandwich panel, in.
b	width of sandwich panel, in.
E	modulus of elasticity of sandwich face sheets, lb/in^2
E_{cx}	effective modulus of elasticity of sandwich core in x-direction, lb/in^2
E_{cy}	effective modulus of elasticity of sandwich core in y-direction, lb/in^2
E_{cz}	effective modulus of elasticity of sandwich core in z-direction, lb/in^2
E22	beam element for which the intrinsic stiffness matrix is given
E43	quadrilateral combined membrane and bending element
G_{cxy}	effective shear modulus of sandwich core in xy-plane, lb/in^2
G_{cxz}	effective shear modulus of sandwich core in xz-plane, lb/in^2
G_{cyz}	effective shear modulus of sandwich core in yz-plane, lb/in^2
h	depth of sandwich panel, in.
h_c	depth of sandwich core, in.
JLOC	joint location (or grid point or node) of finite-element model
m	number of deformation half waves in x-direction
SPAR	structural performance and resizing finite-element computer program
S81	hexahedron (or brick) element
T	temperature, °F
T_l	temperature of lower face sheet, °F

T_u	temperature of upper face sheet for the flat-temperature profile, or temperature of upper-face-sheet plateau zone for the dome-temperature profile, °F
t_s	thickness of sandwich face sheets, in.
w	deflection at arbitrary point of middle plane of sandwich panel, in.
w_{max}	maximum deflection at center of sandwich panel, in.
x, y, z	rectangular Cartesian coordinates, in.
x'	shifted x-coordinate ($x' = x + a/2$), in.
α	coefficient of thermal expansion of solid plate or sandwich face sheets, in/in-°F
α_{cx}	coefficient of thermal expansion of sandwich core in x-direction, in/in-°F
α_{cy}	coefficient of thermal expansion of sandwich core in y-direction, in/in-°F
α_{cz}	coefficient of thermal expansion of sandwich core in z-direction, in/in-°F
α_l	coefficient of thermal expansion of sandwich face sheets at temperature T_l, in/in-°F
α_u	coefficient of thermal expansion of sandwich face sheets at temperature T_u, in/in-°F
ΔT	temperature differential between upper and lower face sheets ($\Delta T = T_u - T_l$), °F
γ_{xz}, γ_{yz}	transverse shear strains of sandwich panel in xz- and yz-plane, in/in.
ν	Poisson ratio of sandwich face sheets
$\nu_{cxy}, \nu_{cxz}, \nu_{cyz}$	Poisson ratios of sandwich core
ρ_{hc}	density of sandwich core, lb/in^3
σ_x	normal stress in x-direction, lb/in^2
σ_y	normal stress in y-direction, lb/in^2
τ_{xy}	shear stress in xy-plane, lb/in^2
τ_{xz}, τ_{yz}	transverse shear stresses in sandwich core in xz- and yz-planes, respectively, lb/in^2

INTRODUCTION

A sandwich panel fabricated with titanium face sheets bonded to titanium honeycomb core through enhanced diffusion bonding process is a potential candidate for application to hypersonic aircraft outer skin structural panels (ref. 1). This type of sandwich structure can operate at elevated temperature levels approaching 1000 °F. When applied as a structural component of hypersonic flight vehicles, this type of sandwich panel is fastened to relatively cool substructures that act as heat sinks. Even under uniform surface heating, the induced panel surface temperature distribution could be nonuniform because of those edge heat sinks. Most analyses do not include the heat sink effects because of added mathematical complexity (refs. 2 through 8). The heated sandwich surface temperature profile is generally a truncated dome shape, with temperature nearly constant in the central plateau zone, tapering down toward the cooler edges. Because the panel is supported by relatively cool substructures and constrained from free expansion, considerable thermal stresses could build up in the panel. The most critical stresses are the compressive stresses. Excessive magnitude of compressive stress built up in the heated face sheet could cause thermal bending caused by thermal moments; thermal buckling; thermal yielding; thermal creep;

thermal crack after cooling down; and other effects. One-sided heating, under certain temperature profiles and edge conditions, also could induce high-intensity transverse shear stress in the sandwich core near the panel corner, which could cause potential shear debonding between the face sheets and the sandwich core. Thus, loss of structural integrity could result.

Ko and Jackson conducted extensive studies, in recent years, concerning the mechanical and thermal buckling characteristics of titanium sandwich panels (refs. 2 through 6) and metal-matrix composite sandwich panels (refs. 7 and 8). Extensive information about thermomechanical buckling characteristics of such sandwich structures have been documented (refs. 2 through 8). To fully understand the thermo-structural response of the sandwich panels in actual applications under which the panel is constrained by the substructures and subjected to one-sided heating, detailed thermal stress analyses are needed to identify the critical stress regions.

This report presents the results of finite-element thermal stress analyses of the sandwich panel under different one-sided heating conditions and edge constraints. The detailed deformation fields and thermal stress fields generated in the sandwich panel are presented graphically for easy visualization of the critical stress regions.

DESCRIPTION OF PROBLEMS

Figure 1 shows the honeycomb-core sandwich panel, which has length a, width b, and depth h (depth of sandwich core h_c). The upper and the lower face sheets have the same thickness of t_s. The panel is subjected to one-sided heating of $\Delta T = T_u - T_l$, the temperature differential between the upper-face-sheet temperature T_u and the lower-face-sheet temperature T_l. The temperature differential ΔT has two types of profiles (i.e., distributions): flat (fig. 2), for which ΔT is constant over the panel surface, and dome shaped (fig. 3), for which ΔT is constant only in the panel central region and decreases linearly to zero at the panel edges. The flat temperature profile heating is for the case when the heat sinks at the panel edges are neglected. The dome-shaped temperature profile heating is for the case when there exist cooler substructures at the panel edges. The temperature profile in figure 3 is actually a truncated pyramid and approximates the actual dome-shaped temperature profile (fig. 4), measured during a thermal ground test of a titanium sandwich panel heated on one side at 10 °F/sec heating rate (ref. 9).

In the thermostructural analysis, the extensional and bending stiffnesses of the sandwich panel were provided by the two face sheets, and the transverse shear stiffness by the sandwich core. The sandwich panel was supported under four edge conditions to study different thermal deformation and thermal stress fields generated in the panel:

1. 4S fixed-edge condition—conventional simply supported edge condition in which the four edges cannot move in the *x*-, *y*-, or *z*-directions.

2. 4S free-edge condition—simply supported edges in which the four edges can move freely in the *x*- and *y*- directions only.

3. 4C fixed-edge condition—conventional clamped edge condition in which the four edges have zero slopes and cannot move in the *x*-, *y*-, or *z*-directions.

4. 4C free-edge condition—clamped edges with zero edge slopes in which the four edges can move freely in the *x*- and *y*-directions only.

3

FINITE-ELEMENT ANALYSIS

This section describes the finite-element models and numerical input values used in the analysis.

Finite-Element Modeling

The structural performance and resizing (SPAR) finite-element computer program (ref. 10) was used in the thermostructural analysis of the sandwich panel. Because the panel is symmetrical with respect to the x- and y-axes (fig. 1), only a quarter-panel was modeled. Figure 5 shows the quarter-panel finite-element model constructed for the sandwich panel. The SPAR constraint commands, SYMMETRY PLANE = 1 and SYMMETRY PLANE = 2, were then used to generate the whole panel for thermostructural analysis. The panel face sheets were modeled with E43 elements (quadrilateral membrane and bending elements), and the sandwich core was modeled with a single layer of S81 elements (hexahedron or brick elements) that connect to the upper- and lower-face-sheet E43 elements.

For the 4S fixed edge (fig. 6(a)) and 4S free edge conditions, the four edges must rotate freely with respect to the corresponding edges of the middle plane. To simulate the 4S boundary condition, pin-ended rigid rods were attached to the panel edge to connect the two face sheets. The midpoints of these rigid rods were pin-jointed to points (fixed or movable in the x- and y-directions) lying in the hypothetical middle plane (fig. 6(a)). Each pin-ended rigid rod was modeled with two identical E22 elements (beam element for which the intrinsic stiffness matrix is given). To simulate the rigidity of the rods, extensional and transverse shear stiffnesses of the E22 elements were made very large. The pin-jointed condition at the face sheet edges was simulated by assigning zero values to the rotational spring constants in the stiffness matrix for the E22 elements. The pin-jointed condition at the hypothetical middle-plane points was simulated by eliminating the three rotational constraints. One node of each E22 element was connected to the associated node of E43 element, and the other node was connected to the hypothetical middle-plane point. The quarter-panel model (fig. 5) for the 4S fixed- and free-edge conditions (to be called 4S model) has 1,299 joint locations (JLOCs), 98 E22 elements for the edge rigid rods, 1,152 E43 elements for the face sheets, and 576 S81 elements for the sandwich core, as shown in the figure.

For the 4C fixed-edge condition (fig. 6(b)), the E22 elements at the panel edges may be neglected. However, when the E22 elements were attached at the panel edges (i.e., using the 4S model) and enforced the zero-edge slopes, the finite-element solutions remained the same as those in which the E22 elements were not used. Retaining the E22 elements requires added computational penalty. For the 4C free-edge condition, the E22 elements were attached at the panel edges to enforce zero-edge slopes and allow free in-plane translations.

Numerical Input Values

The dimensions and the material properties used in this study (tables 1 through 3) are identical to the titanium honeycomb-core sandwich panel previously used in thermostructural simulation tests at NASA Dryden Flight Research Center (ref. 9).

Table 1. Geometry of a panel.

$$a = b = 24 \text{ in.}$$
$$h = 0.75 \text{ in.}$$
$$t_s = 0.06 \text{ in.}$$

Table 2. Face sheet properties.

	200 °F	900 °F
E, lb/in^2	15.4×10^6	13.1×10^6
ν	0.31	0.31
α, in/in-°F	4.3×10^{-6}	5.35×10^{-6}

Table 3. Honeycomb core (properties at 600 °F).

E_{cx}	$= 2.7778 \times 10^4$	lb/in^2
E_{cy}	$= 2.7778 \times 10^4$	lb/in^2
E_{cz}	$= 2.7778 \times 10^5$	lb/in^2
G_{cxy}	$= 0.00613$	lb/in^2
G_{cyz}	$= 0.81967 \times 10^5$	lb/in^2
G_{cxz}	$= 1.81 \times 10^5$	lb/in^2
ν_{cxy}	$= 0.658 \times 10^{-2}$	
ν_{cyz}	$= 0.643 \times 10^{-6}$	
ν_{cxz}	$= 0.643 \times 10^{-6}$	
α_{cx}	$= 5.37 \times 10^{-6}$	in/in-°F
α_{cy}	$= 5.37 \times 10^{-6}$	in/in-°F
α_{cz}	$= 5.37 \times 10^{-6}$	in/in-°F
ρ_{hc}	$= 3.674 \times 10^{-3}$	lb/in^3

The temperature loadings on the sandwich panel are $T_u = 900$ °F for the upper face sheets (entire regions (fig. 2) or central regions (fig. 3)) and $T_l = 200$ °F for the lower face sheet.

DISPLACEMENT FIELD

A theoretical equation describing the displacement field of a solid rectangular plate was modified to make it applicable to sandwich panels. This equation was required to evaluate the transverse shear effect on the sandwich panel deflection.

The following equation, taken from reference 11, describes the deflection field of a simply supported solid isotropic rectangular plate under differential heating.

$$w(x', y) = -\frac{4\alpha\Delta T a^2(1+\nu)}{\pi^3 h} \sum_{m=1,3,5,\dots}^{\infty} \frac{\sin\frac{m\pi x'}{a}}{m^3}\left(1 - \frac{\cosh\frac{m\pi y}{a}}{\cosh\frac{m\pi b}{2a}}\right) \qquad (1)$$

where the origin of the coordinates for this equation is at $x = -a/2$, $y = 0$; namely,

$$x' = x + \frac{a}{2} \qquad (2)$$

When the transverse shear effect of the sandwich core is neglected (i.e., $\gamma_{xz} = \gamma_{yz} = 0$), the sandwich panel behaves like a solid plate, and therefore, the above equation could be used to approximate the deflection field of the sandwich plate. The validity of equation (1) is addressed later in the "Results" section. To apply equation (1) for the sandwich plate, the thermal bending term $\alpha\Delta T$ must be replaced with

$$\alpha\Delta T = \alpha_u T_u - \alpha_l T_l \qquad (3)$$

The displacement field calculated from equation (1) using equation (3), is then compared with that calculated from the finite-element method for only the case when the transverse shear effect of the sandwich core is neglected.

RESULTS

Displacements

Figures 7(a) and 7(b) show the half-panel plots of the deformed shapes of the sandwich panel under different edge conditions subjected to flat temperature profile heating. These half-panel plots were generated from the quarter-panel plots by using the SYMMETRY command. The panel's deformed shapes under fixed and free edges are the same; however, as will be seen later, the induced thermal stress fields are quite different. Notice that under the 4C edge condition (fixed or free, fig. 7(b)), the panel deflection is zero (i.e., the deformed panel remains flat).

Figures 8(a) and 8(b) show the similar half-panel plots for the case when the heating is of the dome-shaped temperature profile. Again, the deformed shapes for the fixed- and free-edge cases are identical. Unlike the previous case, the panel deflection away from the boundaries under the 4C edge condition, fixed or free, (fig. 8(b)) is nonzero.

Figure 9 shows the deflection curves of the sandwich panel's middle plane center line, along the x-axis, for different heating cases. The figure also shows the deflection curve calculated from equation (1) up to 10 terms summation for flat temperature profile heating. The deflection curve calculated from equation (1) falls pictorially on that calculated from the finite-element method (for the flat temperature case) neglecting the transverse shear effect (i.e., by setting $\gamma_{xz} = \gamma_{yz} = 0$, namely by making G_{cxz} and G_{cyz} very large). The maximum deflection at the center of sandwich panel middle plane w_{max} calculated from equation (1) using 10-terms series summation is $w_{max} = 0.2931$ in., and that calculated from the finite-element method (for $\gamma_{xz} = \gamma_{yz} = 0$) is $w_{max} = 0.2920$ in. The close correlation between

6

these two values gives confidence in the applicability of equation (1) for the sandwich panel, and also in the adequacy of the finite-element model used.

The deflection equation (1) and the finite-element models were also used to study the effect of transverse shear on panel deflections. Table 4 lists the panel maximum deflections w_{max} for different heating and edge conditions. The w_{max} values in parentheses are applicable when the transverse shear effect is neglected (i.e., $\gamma_{xz} = \gamma_{yz} = 0$). The w_{max} value calculated from equation (1) (10 terms summation) is also shown in brackets for comparison. Notice that by neglecting the transverse shear effect, the panel deflection could be underpredicted by 3 to about 11 percent depending on the edge and heating conditions. In practical application, the panel is under dome temperature profile heating and 4C edge condition (closer to fixed edges rather than free edges). For this case, the maximum deflection is only $w_{max} =$ 0.0576 in. Such a small panel deflection greatly minimizes any concern that the deformed panel could severely disturb the airflow field and, therefore, alter the surface heating rate.

Table 4. Maximum deflections at center of sandwich panel's middle plane; $T_u = 900$ °F, $T_l = 200$ °F.

Temperature profile	w_{max}, in.			
	4S fixed	4S free	4C fixed	4C free
Flat	0.3305	0.3305	0	0
	(0.2920)	(0.2920)	– – –	– – –
	[0.2931]	– – –	– – –	– – –
Dome	0.3050	0.3050	0.0576	0.0576
	(0.2745)	(0.2745)	(0.0557)	(0.0557)

Thermal Stresses

This section presents thermal stress results for flat and dome-shaped temperature heating applied to the sandwich panel under the various edge conditions.

Flat Temperature Profile

Upper Face Sheet
Figures 10 through 21 show various distributions of normal stresses $\{\sigma_x, \sigma_y\}$, which are negative (i.e., compression), and the shear stress (τ_{xy}), in the upper face sheet of the sandwich panel induced by flat-temperature-profile heating. Again, these half-panel plots were generated from quarter-panel plots using the SYMMETRY command. The figures show the peak stress points and values of peak stress. For the 4S fixed- and free-edge cases, the distributions of $\{\sigma_x, \sigma_y\}$ (figs. 10, 11, 13, and 14) are slightly saddle shaped, and the peak compression points of $\{\sigma_x, \sigma_y\}$ are at the midpoints of the panel edges, $y = b/2$

and $x = a/2$, respectively. The distributions of the shear stress τ_{xy} in the upper face sheet for the 4S fixed- and free-edge cases (figs. 12 and 15) are distorted bell-shaped within each quarter-panel region. The magnitude of τ_{xy} reaches its peak value near the panel corners and decreases steeply to zero at the panel edges and rapidly to zero at the two axes of symmetry. By freeing the panel edges from the fixed constraint, the magnitudes of compressive stresses $\{\sigma_x, \sigma_y\}$ could be reduced considerably (figs. 10, 11, 13, and 14); however, the distributions of shear stress τ_{xy} remained almost the same (figs. 12 and 15). For the 4C fixed-edge case, the compressive stresses $\{\sigma_x, \sigma_y\}$ in the upper face sheet (figs. 16 and 17) are constant everywhere, and the shear stress τ_{xy} is zero everywhere (fig. 18). For the 4C free-edge case, the compressive stresses $\{\sigma_x, \sigma_y\}$ are almost constant over the upper face sheet (figs. 19 and 20), and the shear stress τ_{xy} induced in the upper face sheet (fig. 21) is nearly zero.

Lower Face Sheet

Figures 22 through 33 show various distributions of $\{\sigma_x, \sigma_y, \tau_{xy}\}$ induced in the lower face sheet of the sandwich panel under different edge conditions for flat-temperature-profile heating. For the fixed-edge cases (4S and 4C), $\{\sigma_x, \sigma_y\}$ are negative (i.e., compression); however, for the free-edge cases (4S and 4C), $\{\sigma_x, \sigma_y\}$ are positive (i.e., tension). For the 4S fixed-edge case, the peak compression points of $\{\sigma_x, \sigma_y\}$ (figs. 22 and 23) are no longer located at the edge midpoints like the upper-face-sheet case (figs. 10 and 11). For the 4S free-edge case, similar to the upper-face-sheet case for which $\{\sigma_x, \sigma_y\}$ are negative (figs. 13 and 14), the peak tensile stress points of $\{\sigma_x, \sigma_y\}$ (figs. 25 and 26), are at the midpoints of the panel edges. The distributions of shear stress τ_{xy} in the lower face sheet for the 4S fixed- and free-edge cases (figs. 24 and 27) are very similar to those for the upper-face-sheet case (figs. 12 and 15); however, the sign of τ_{xy} is reversed. For the 4C fixed-edge case, the compressive stresses $\{\sigma_x, \sigma_y\}$ are identical and constant everywhere in the lower face sheet (figs. 28 and 29), but the magnitude is much lower than that in the upper face sheet (figs. 16 and 17), and the shear stress τ_{xy} in the lower face sheet (fig. 30), like the upper face sheet case (fig. 18), is zero everywhere. For the 4C free-edge case, $\{\sigma_x, \sigma_y\}$ in the lower face sheet are both positive and nearly constant (figs. 31 and 32), and the shear stress τ_{xy} induced in the lower face sheet (fig. 33) is at an insignificant level similar to the case for the upper face sheet (fig. 21).

Sandwich Core

Figures 34 and 35 show the distributions of transverse shear stresses $\{\tau_{xz}, \tau_{yz}\}$ induced in the sandwich core under 4S fixed- or 4S free-edge condition subjected to flat-temperature-profile heating. Each transverse shear stress value used in the plots is the average of the eight stress values at the eight nodes of the S81 element. Both the 4S fixed- and 4S free-edge cases induced identical transverse shear stresses. The shape of τ_{xz} plot (fig. 34) is like an airplane wing with winglets; for τ_{yz} (fig. 35) the shape is like fox ears near the panel's edge. The values of $\{\tau_{xz}, \tau_{yz}\}$ are quite low in the core central region and rises steeply to their respective peak values at the corners of the core (i.e., the transverse shear stress concentrations occur at the panel's corners). The levels of $\{\tau_{xz}, \tau_{yz}\}$ stress concentrations are relatively low; however, they might cause the thin honeycomb walls to buckle in shear.

Under flat-temperature-profile heating, both the 4C fixed- and 4C free-edge cases induced no transverse shear stresses $\{\tau_{xz}, \tau_{yz}\}$ in the sandwich core, as shown in figures 36 and 37. For actual

8

application, the panel's edge condition is closer to the 4C fixed-edge condition, which induces no transverse shears. Therefore, under the present heating level, no concern about stress concentration caused by transverse shear is warranted.

Dome Temperature Profile

Upper Face Sheet
Figures 38 through 49 show the distributions of $\{\sigma_x, \sigma_y, \tau_{xy}\}$ in the upper face sheet of the sandwich panel induced by the dome-temperature-profile heating. The distributions of the compressive stresses $\{\sigma_x, \sigma_y\}$ for the 4S fixed- and free-edge cases (figs. 38, 39, 41, and 42) and 4C fixed- and free-edge cases (figs. 44, 45, 47, and 48), are hat shaped, reflecting partly the shape of the dome temperature profile. Unlike the flat-temperature-profile case, the peak compression points of $\{\sigma_x, \sigma_y\}$ are now at the boundary of the central plateau zone and not at the panel's edges. The shear stress distributions for the 4S fixed- and free-edge cases (figs. 40 and 43) are similar to those of the flat-temperature-profile case (figs. 12 and 15) but with slightly higher peak magnitudes. For the 4C fixed- and free-edge cases, the shear stress τ_{xy} (figs. 46 and 49), is zero only at the two axes of symmetry and the panel's corners (the plotted corner points are not exactly at the panel's corners, and therefore, show finite values) but nonzero at the panel edges because of the nonuniform thermal expansions. The peak magnitudes of τ_{xy} are lower than those for the 4S fixed- and free-edge cases (figs. 40 and 43) and are in the vicinity of the panel's corners.

Lower Face Sheet
Figures 50 through 61 show various distributions of $\{\sigma_x, \sigma_y, \tau_{xy}\}$ in the lower face sheet induced by the dome-temperature-profile heating. The stress distributions are very similar to those for the flat temperature profile and, unlike the upper face sheet, they do not reflect the dome temperature profile. Those figures also indicate the peak stress points. For the 4C fixed and 4C free cases (figs. 56 through 61), the distributions of $\{\sigma_x, \sigma_y, \tau_{xy}\}$ stresses in the lower face sheets are slightly wavy in shape with peak stress points at the edges.

Sandwich Core
Figures 62 and 63, respectively, show the distributions of transverse shear stresses $\{\tau_{xz}, \tau_{yz}\}$ induced in the sandwich core for the 4S fixed- and 4S free-edge cases under dome-temperature-profile heating. Both the 4S fixed- and 4S free-edge case give identical $\{\tau_{xz}, \tau_{yz}\}$ distributions. The τ_{xz} plot (fig. 62) also looks like an airplane wing with winglets, and the τ_{yz} plot (fig. 63) looks like cat ears near the panel's edge. The peak magnitudes of $\{\tau_{xz}, \tau_{yz}\}$ are now at the core edges and near the core corners—not exactly at the core corners like the previous case. The $\{\tau_{xz}, \tau_{yz}\}$ stress concentrations are less severe for the dome-temperature-profile case (figs. 62 and 63), as compared with the flat-temperature-profile case (figs. 34 and 35). For dome-temperature-profile heating, the magnitudes of transverse stresses $\{\tau_{xz}, \tau_{yz}\}$ induced in the sandwich core under both 4C fixed- and 4C free-edge conditions (figs. 64 through 67) are quite close and very small—not exactly zero like for flat-temperature-profile heating (figs. 36 and 37).

Peak Stress Summary

Table 5 lists the peak values of the thermal stresses $\{\sigma_x, \sigma_y, \tau_{xy}\}$ (positive or negative) induced in the upper and lower face sheets of the sandwich panel. Table 6 lists the peak values of the transverse shear stresses $\{\tau_{xz}, \tau_{yz}\}$ induced in the sandwich core.

Table 5. Peak thermal stresses in face sheets of sandwich panel; T_u = 900 °F, T_l = 200 °F (yield stress = 126,000 lb/in^2).

	Upper face sheet					
	Flat temperature profile			Dome temperature profile		
Edge condition	σ_x, lb/in^2	σ_y, lb/in^2	τ_{xy}, lb/in^2	σ_x, lb/in^2	σ_y, lb/in^2	τ_{xy}, lb/in^2
4S fixed	−89,245	−87,430	23,827	−75,961	−75,796	28,579
4S free	−26,161	−25,783	23,904	−26,140	−25,576	30,917
4C fixed	−107,470	−107,470	0	−96,192	−96,087	12,984
4C free	−46,177	−45,801	219	−45,488	−44,996	14,062
	Lower face sheet					
4S fixed	−62,948	−64,010	23,827	−53,433	−54,553	19,242
4S free	25,671	22,931	23,755	21,084	18,251	17,086
4C fixed	−19,190	−19,190	0	−29,399	−28,160	2,115
4C free	44,339	44,393	219	36,994	36,743	2,757

Table 6. Peak transverse shear stresses in sandwich core; T_u = 900 °F, T_l = 200 °F.

	Flat temperature profile		Dome temperature profile	
Edge condition	τ_{xz}, lb/in^2	τ_{yz}, lb/in^2	τ_{xz}, lb/in^2	τ_{yz}, lb/in^2
4S fixed	2,216	1,798	1,339	1,065
4S free	2,216	1,798	1,339	1,065
4C fixed	0	0	134	86
4C free	0	0	142	88

CONCLUSIONS

Finite-element thermal stress analyses were performed on a titanium honeycomb-core sandwich panel supported at its edges under four different edge conditions, and heated on one side under both flat and dome-shaped temperature profiles. Detailed deformation and thermal stress fields induced in the

sandwich panel were presented graphically for easy visualization. The key results of the thermostructural analyses are as follows:

1. If the transverse shear effect of a sandwich core is neglected, the maximum deflection of the sandwich panel was underpredicted by 3 to about 11 percent, depending on edge conditions and heating temperature profiles.

2. Under the flat-temperature-profile heating:

   (a) The classical deflection equation for a simply supported rectangular flat plate adequately describes the deformation field of a simply supported sandwich panel for which the transverse shear effect of the sandwich core is neglected, as validated by the finite-element solutions.

   (b) For the 4S fixed- and 4S free-edge conditions, the peak stress points of the normal stresses $\{\sigma_x, \sigma_y\}$ are at the edges of the face sheets; the peak stress points of the shear stress τ_{xy} are at the diagonal lines and near the corners of the face sheets; and the peak stress points of the transverse shear stresses $\{\tau_{xz}, \tau_{yz}\}$ are right at the corners of the sandwich core.

   (c) For the 4C fixed-edge condition, the normal stresses $\{\sigma_x, \sigma_y\}$ in both of the face sheets are constant everywhere, and the shear stress τ_{xy} in both of the face sheets is zero everywhere. For the 4C free-edge condition, the normal stresses $\{\sigma_x, \sigma_y\}$ in both of the face sheets are almost constant, and the shear stress τ_{xy} in both of the face sheets is negligibly low. For both 4C fixed- and 4C free-edge conditions, the transverse shear stresses $\{\tau_{xz}, \tau_{yz}\}$ are zero everywhere in the sandwich core.

3. Under the dome-temperature-profile heating:

   (a) For all four edge conditions, the peak stress points of normal stresses $\{\sigma_x, \sigma_y\}$ in the upper face sheet are at the boundary of the temperature plateau zone—not at the face sheet edges. The peak stress points of the shear stress τ_{xy} in the upper face sheet (for all the edge conditions) and in the lower face sheet (for 4S fixed- and 4S free-cases only) are on the diagonal lines and near the corners of the face sheets.

   (b) The distributions of $\{\sigma_x, \sigma_y\}$ in the lower face sheet for the 4S fixed and 4S free cases are very similar to those for the flat-temperature-profile case and do not reflect the temperature profile applied to the upper face sheet. For the 4C fixed and 4C free cases, the distributions of $\{\sigma_x, \sigma_y, \tau_{xy}\}$ stresses in the lower face sheets are slightly wavy in shape with peak stress points at the edges of the lower face sheet.

   (c) For 4S fixed and 4S free cases, the peak stress points of the transverse shear stresses $\{\tau_{xz}, \tau_{yz}\}$ in the sandwich core are at the core edges and very near the core corners. For the 4C fixed and 4C free cases, the transverse shear stresses $\{\tau_{xz}, \tau_{yz}\}$ induced in the sandwich core have extremely low magnitudes.

REFERENCES

1. Tenney, D.R., W.B. Lisagor, and S.C. Dixon, "Materials and Structures for Hypersonic Vehicles," *J. Aircraft*, vol. 26, no. 11, November 1989, pp. 953–970.

2. Ko, William L. and Raymond H. Jackson, *Thermal Behavior of a Titanium Honeycomb-Core Sandwich Panel*, NASA TM-101732, January 1991.

3. Ko, William L. and Raymond H. Jackson, "Combined Compressive and Shear Buckling Analysis of Hypersonic Aircraft Structural Sandwich Panels," AIAA Paper No. 92-2487-CP, presented at the 33rd AIAA/ASME/ASCE/AHS/ASC Structures, Structural Dynamics and Materials Conference, Dallas, Texas, April 13–15, 1992; NASA TM-4290, May 1991.

4. Ko, William L., "Mechanical and Thermal Buckling Analysis of Sandwich Panels Under Different Edge Conditions," *Proc. 1st Pacific International Conference on Aerospace Science and Technology*, Tainan, Taiwan, Dec. 6–9, 1993.

5. Ko, William L., *Mechanical and Thermal Buckling Analysis of Rectangular Sandwich Panels Under Different Edge Conditions*, NASA TM-4585, April 1994.

6. Ko, William L., *Predictions of Thermal Buckling Strengths of Hypersonic Aircraft Sandwich Panels Using Minimum Potential Energy and Finite Element Methods*, NASA TM-4643, May 1995.

7. Ko, William L. and Raymond H. Jackson, *Combined-Load Buckling Behavior of Metal-Matrix Composite Sandwich Panels Under Different Thermal Environments*, NASA TM-4321, September 1991.

8. Ko, William L. and Raymond H. Jackson, "Compressive and Shear Buckling Analysis of Metal Matrix Composite Sandwich Panels Under Different Thermal Environments," *Composite Structures*, vol. 25, July 1993, pp. 227–239. Also NASA TM-4492, June 1993.

9. Richards, W. Lance and Randolph C. Thompson, "Titanium Honeycomb Panel Testing," *Proceedings Structural Testing Technology at High Temperature Conference*, Dayton, Ohio, Nov. 4–6, 1991, Society for Experimental Mechanics, Inc., June 1992.

10. Whetstone, W.D., *SPAR Structural Analysis System Reference Manual, System Level 13A, vol. 1, Program Execution*, NASA CR-158970-1, December 1978.

11. Timoshenko, S. and S. Woinowsky-Krieger, *Theory of Plates and Shells*, McGraw-Hill Book Co., Inc., New York, 1959, p. 164.
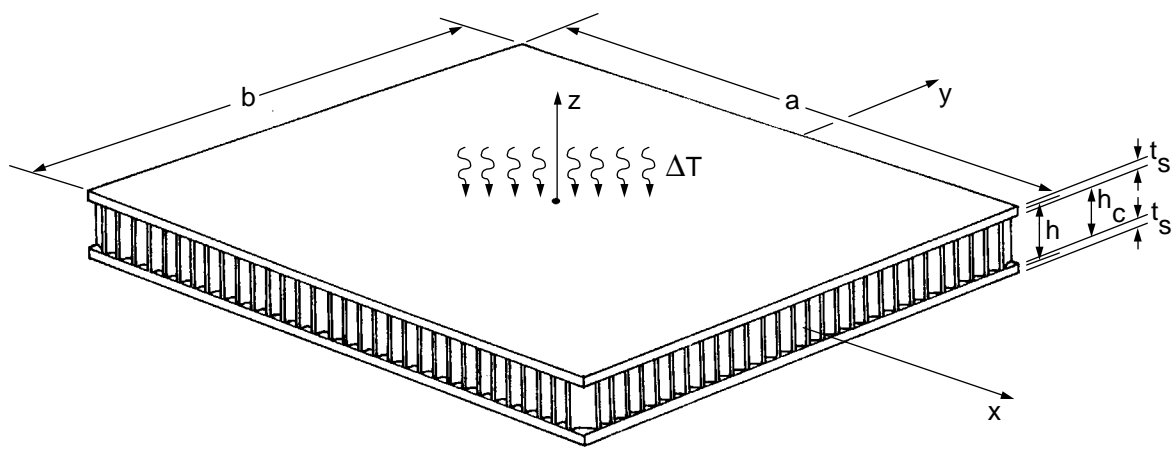
Figure 1. Honeycomb-core sandwich panel under one-sided thermal loading.

960440

13
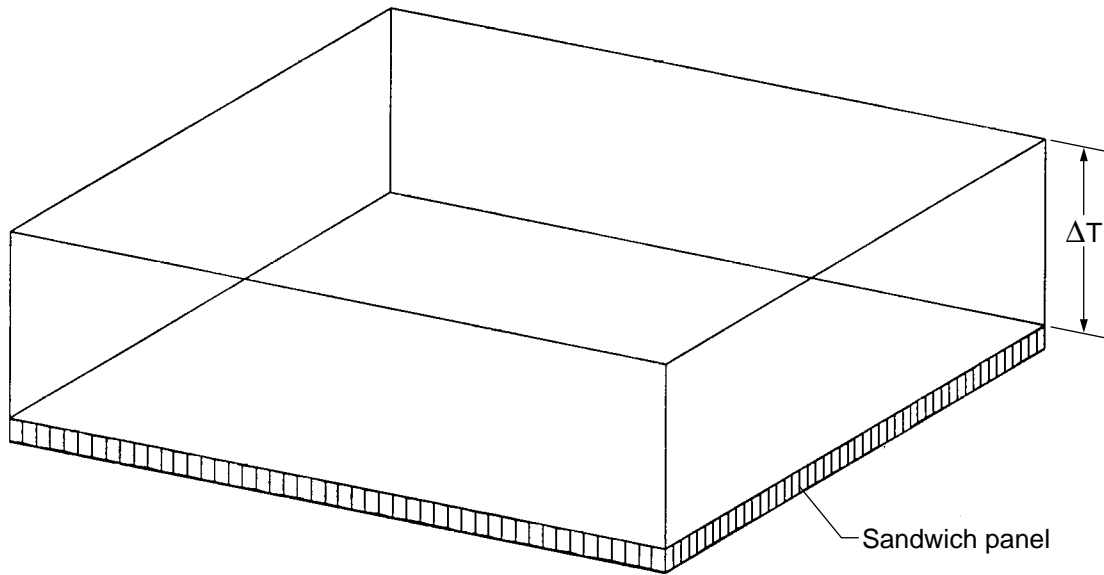
Figure 2. Heating under flat temperature profile; $\Delta T = T_u - T_l$.
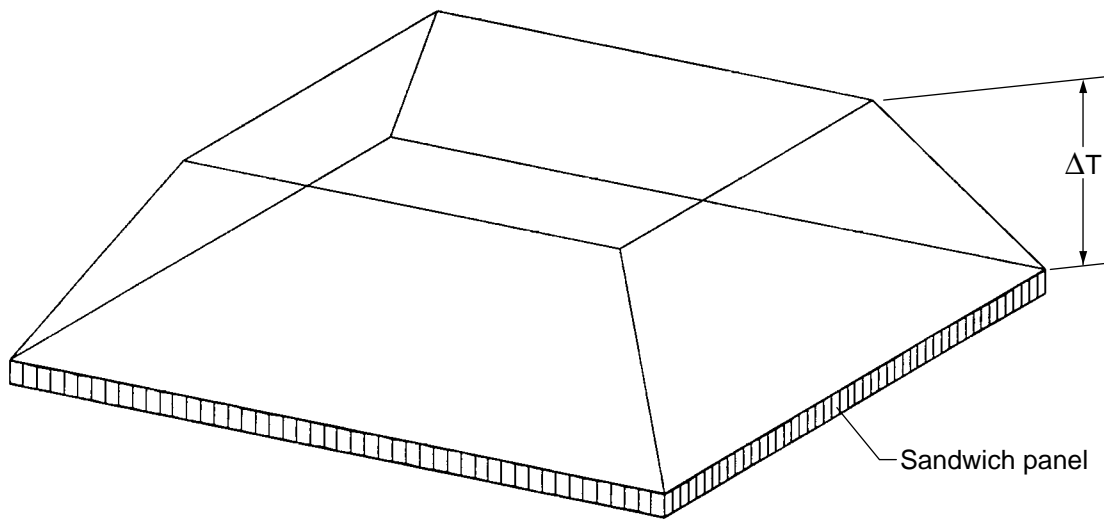
Figure 3. Heating under dome temperature profile; $\Delta T = T_u - T_l$.
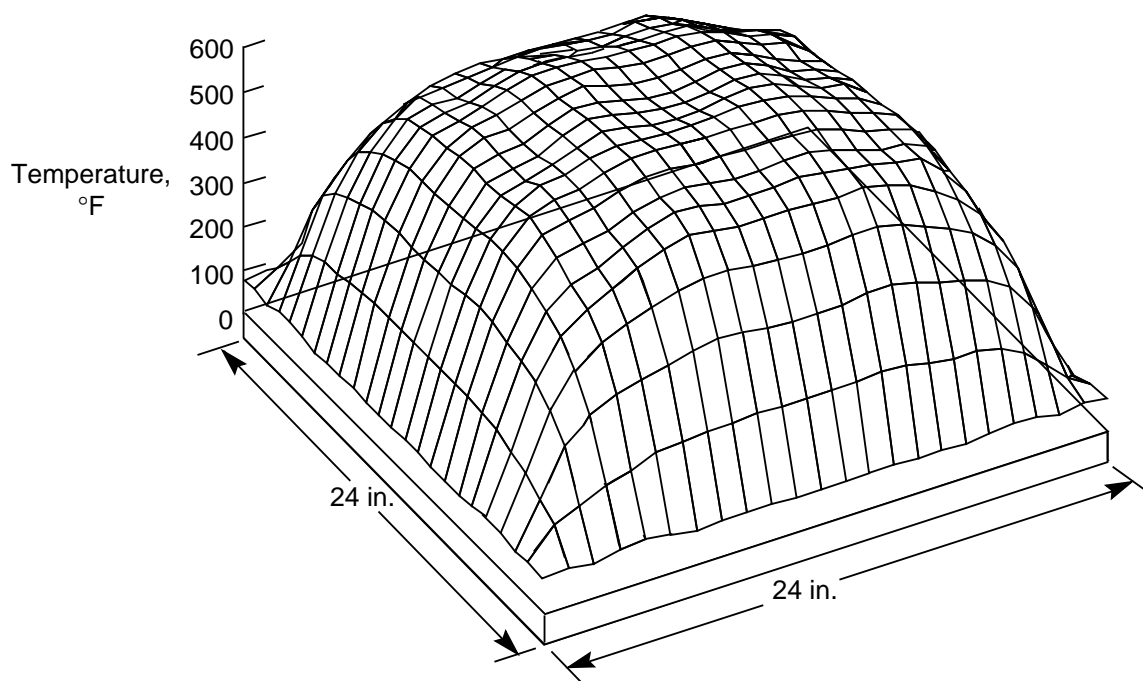
Figure 4. Measured temperature distribution in upper surface of titanium honeycomb-core sandwich panel, heated on upper side at 10 °F/sec heating rate, with four edges supported by test fixtures (heat sink).

15

JLOC   1299
E22 elements   98
E43 elements   1152
S81 elements   576
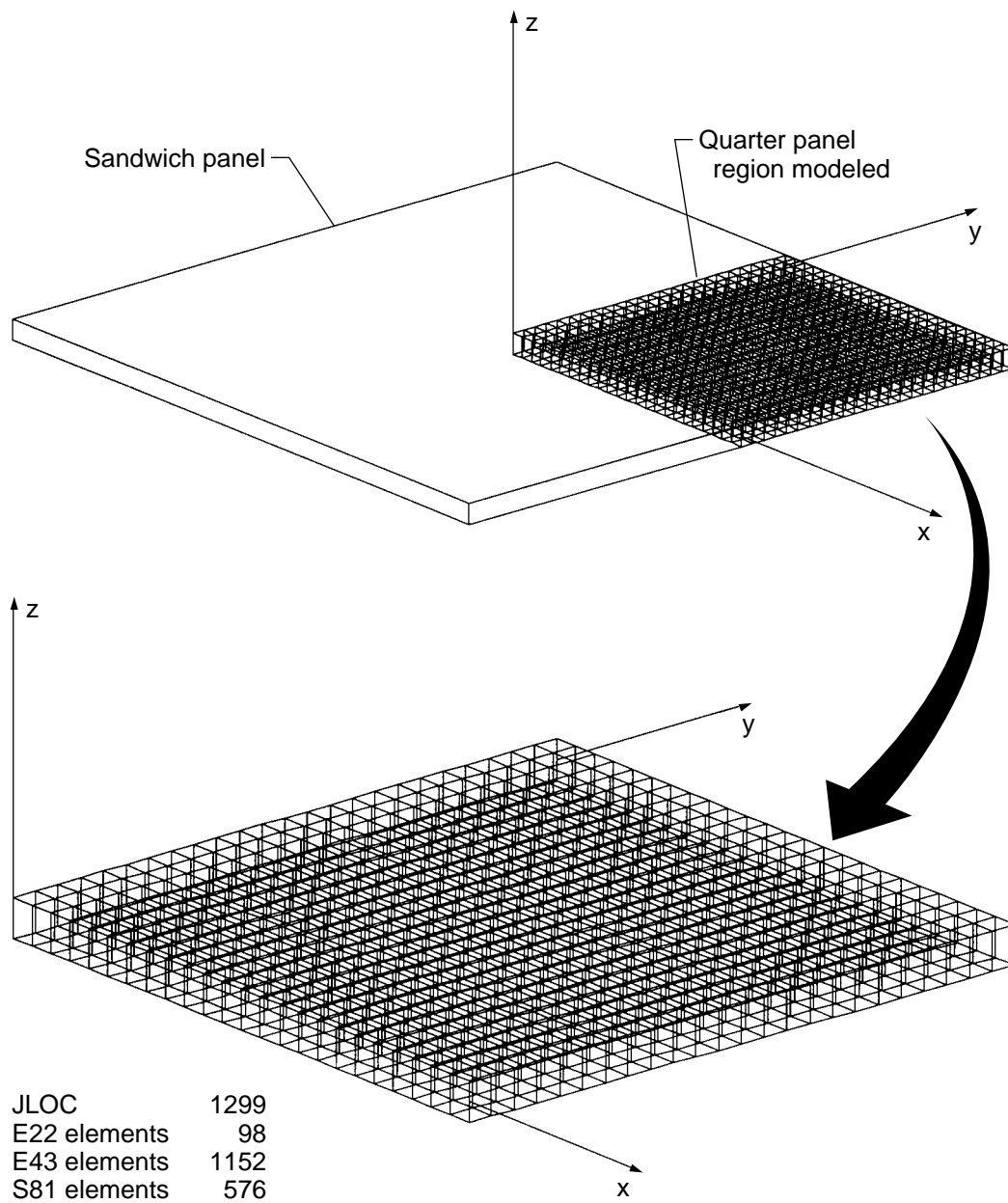
970047

Figure 5. Quarter-panel, finite-element model for sandwich panel.

○ : Pin joint

Rigid bar

Maximum γ_{xz}

x

z

E43

E22

S81

S81

E22

E43

960443

(a) 4S edge condition (fixed).

Zero slope, $\gamma_{xz} = 0$

x

z

E43

S81

S81

E43

960444
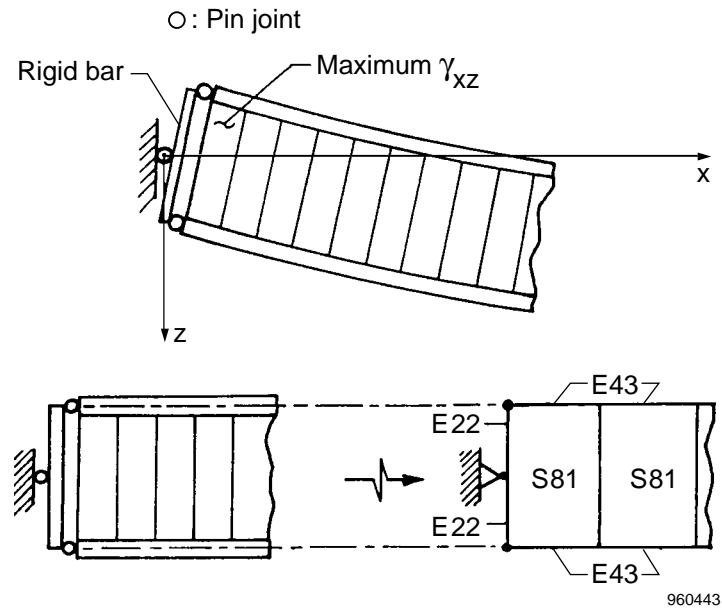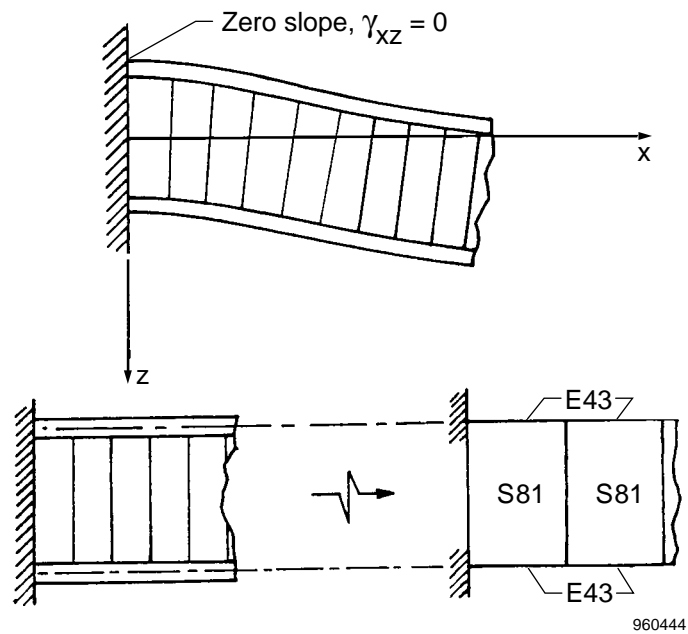
(b) 4C edge condition (fixed).

Figure 6. Simulation of different edge conditions.

960445

(a) 4S edge condition (fixed and free).

960446
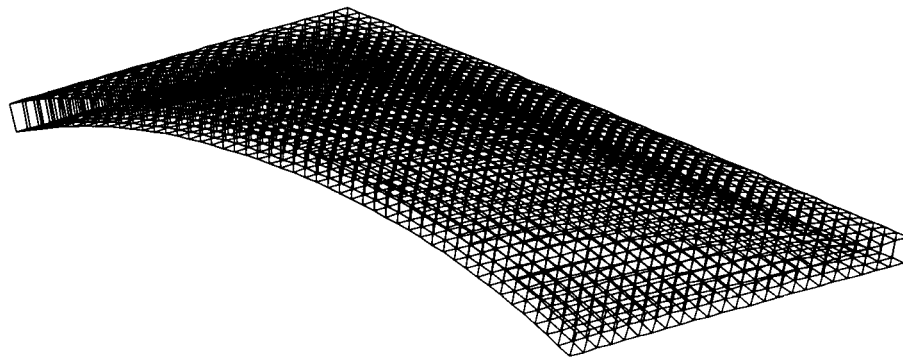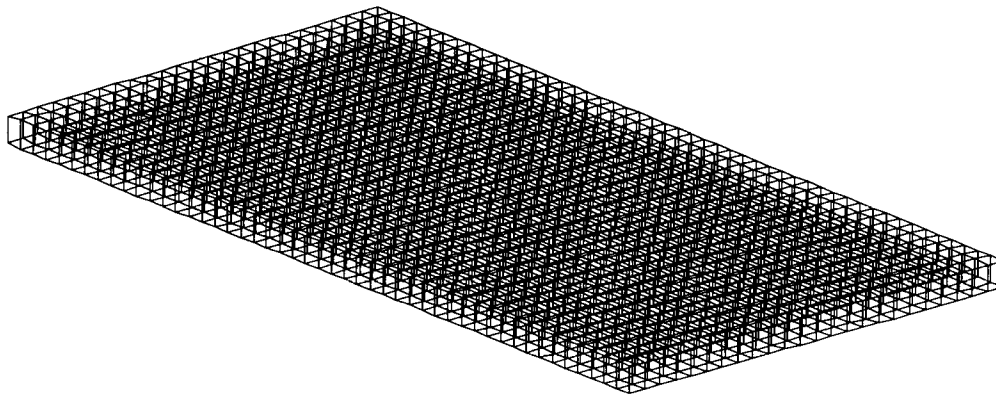
(b) 4C edge condition (fixed and free).

Figure 7. Deformed shapes of sandwich panel under heating on one side; flat temperature profile; T_u = 900 °F, T_l = 200 °F; half-panel plots.

960447

(a) 4S edge condition (fixed and free).

960448
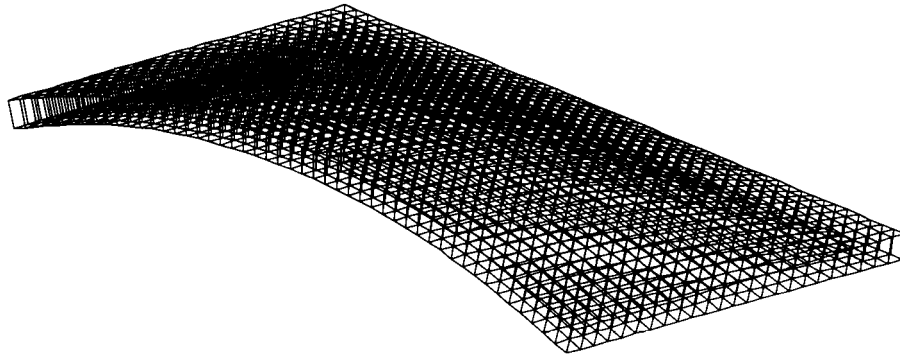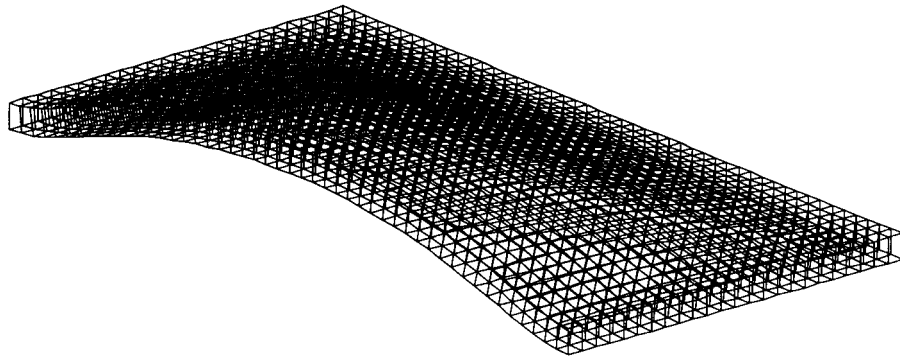
(b) 4C edge condition (fixed and free).

Figure 8. Deformed shapes of sandwich panel under heating on one side; dome temperature profile; T_u = 900 °F, T_l = 200 °F; half-panel plots.
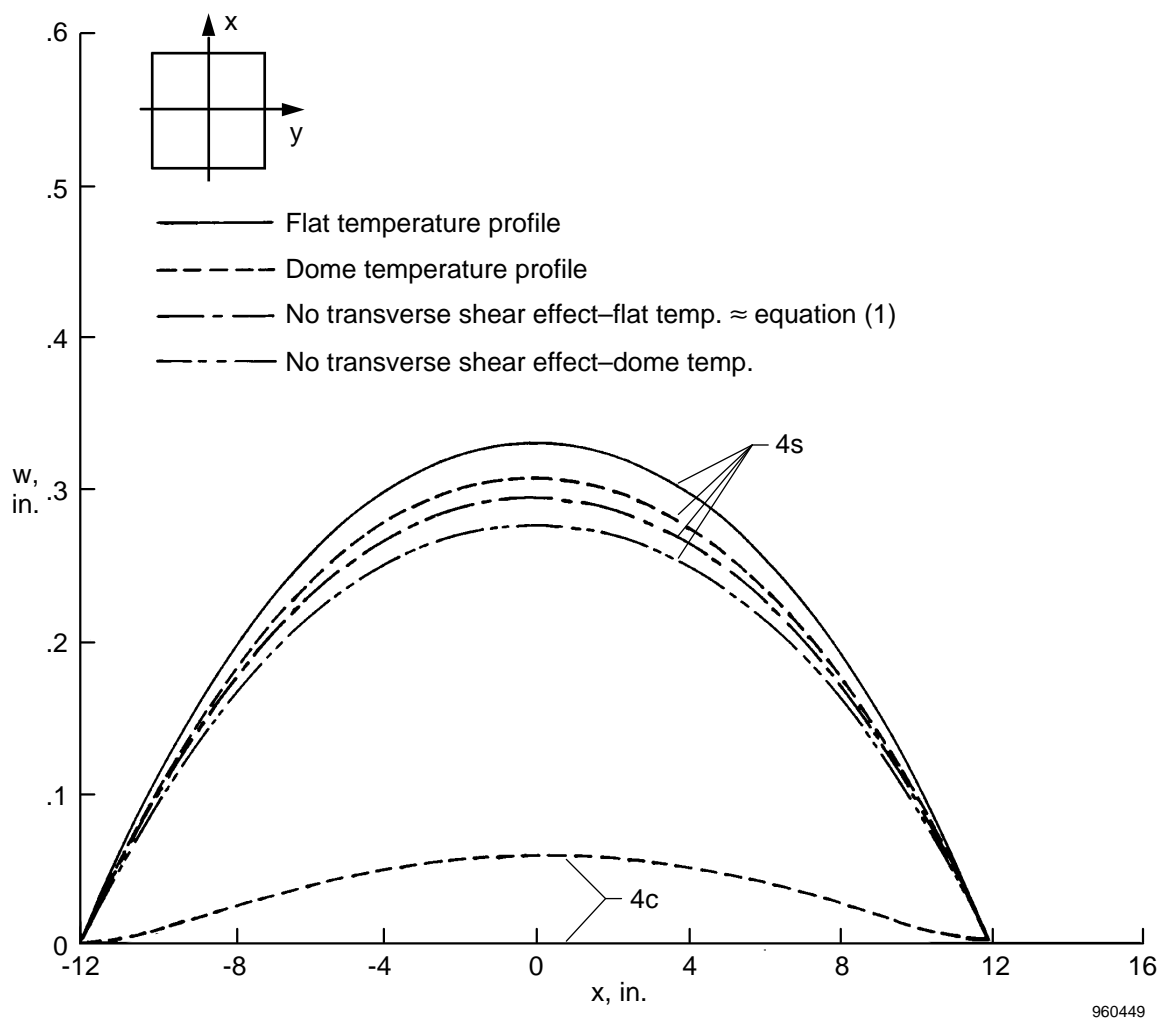
Figure 9. Deflections of sandwich panel's middle plane along x-axis; $T_u = 900$ °F, $T_l = 200$ °F.

Normal and Shear Stress Distributions in Upper Face Sheet—Flat Temperature Profile
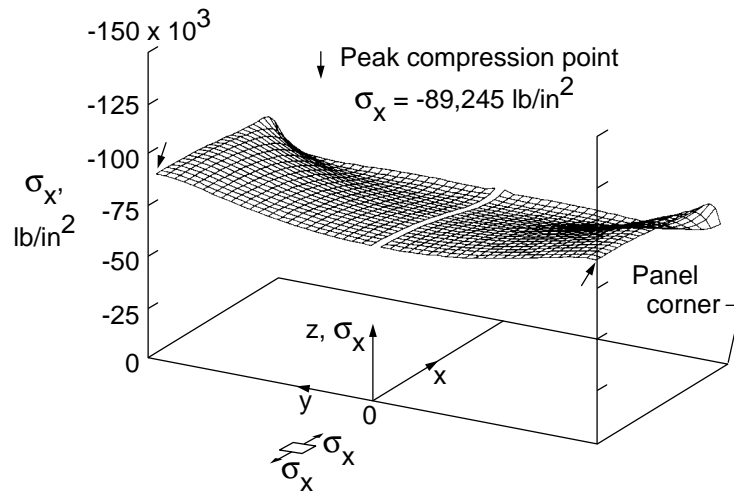
Figure 10. Distribution of σ_x in the upper face sheet; 4S fixed-edge condition; flat temperature profile; $T_u = 900$ °F, $T_l = 200.$ °F.
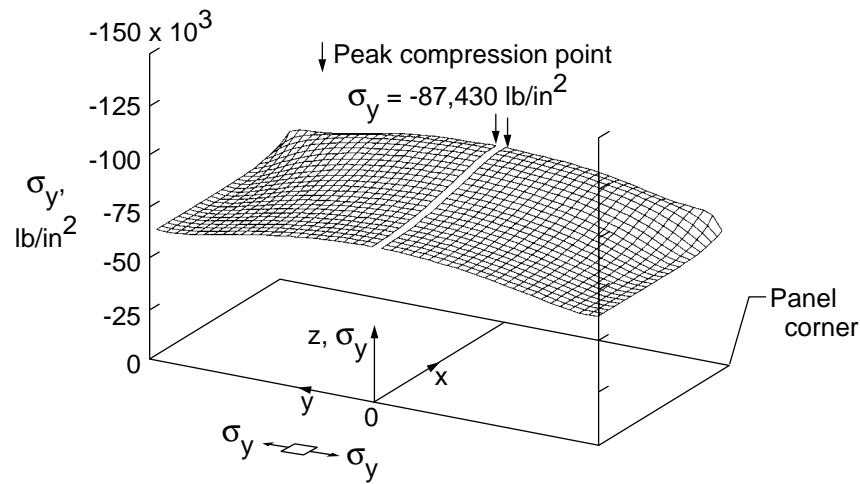
Figure 11. Distribution of σ_y in the upper face sheet; 4S fixed-edge condition; flat temperature profile; $T_u = 900$ °F, $T_l = 200$ °F.
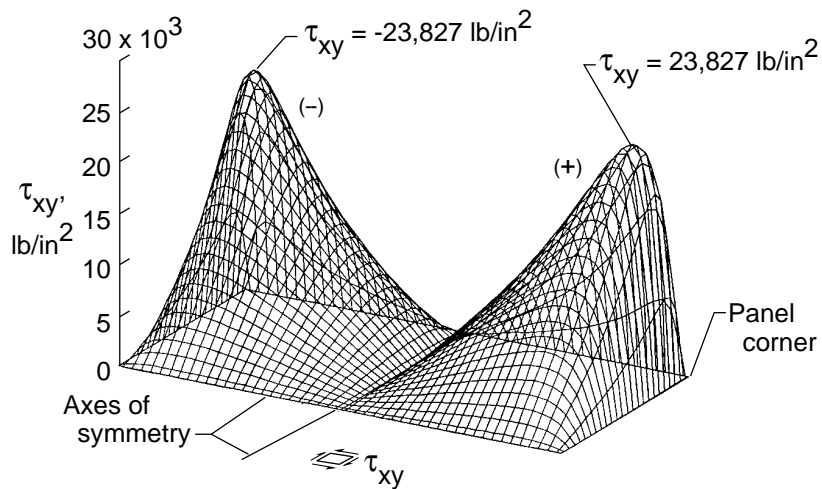
Figure 12. Distribution of τ_{xy} in the upper face sheet; 4S fixed-edge condition; flat temperature profile; $T_u = 900$ °F, $T_l = 200$ °F.

22
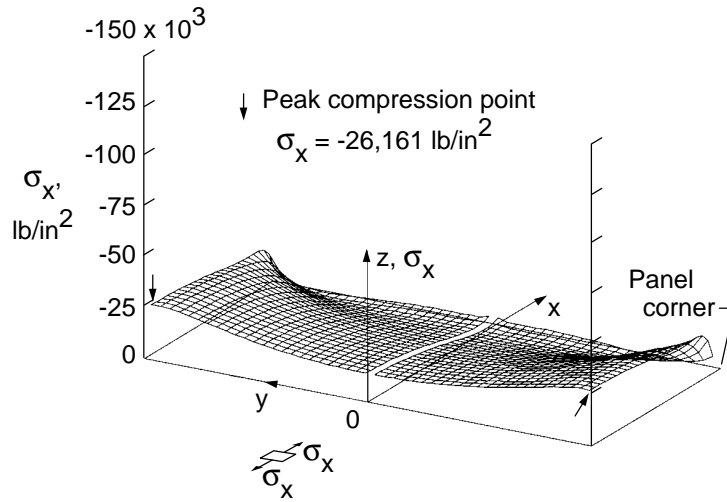
960453

Figure 13. Distribution of σ_x in the upper face sheet; 4S free-edge condition; flat temperature profile; $T_u = 900\ °\text{F}$, $T_l = 200\ °\text{F}$.
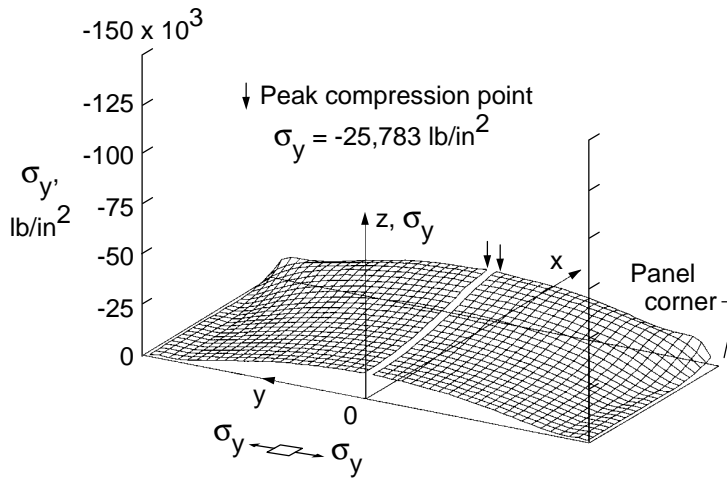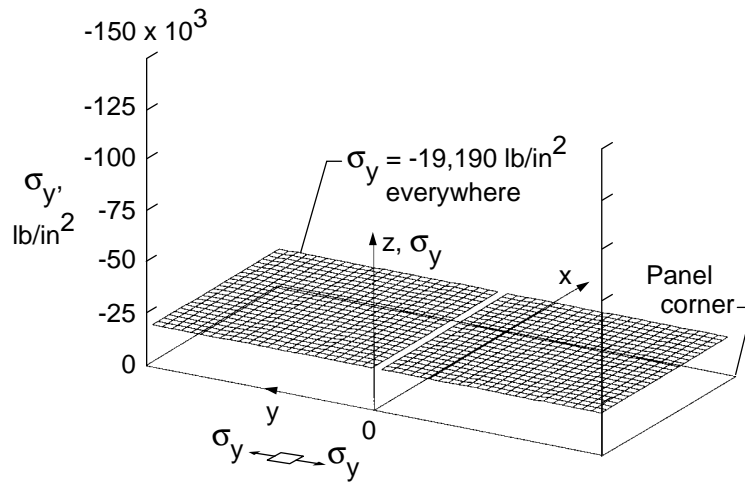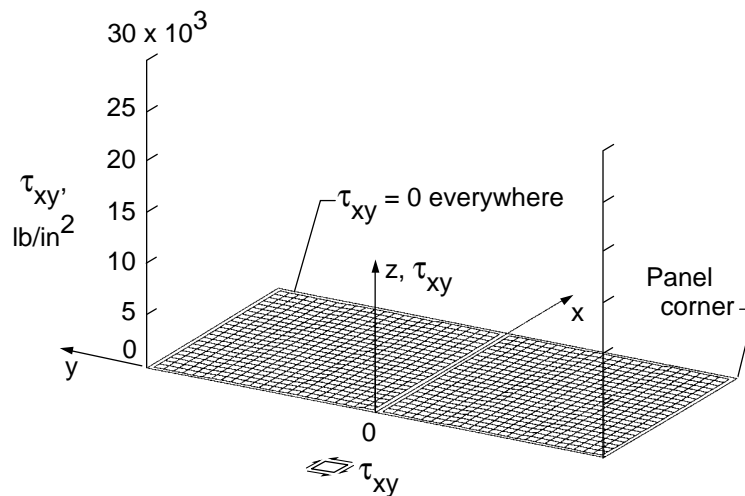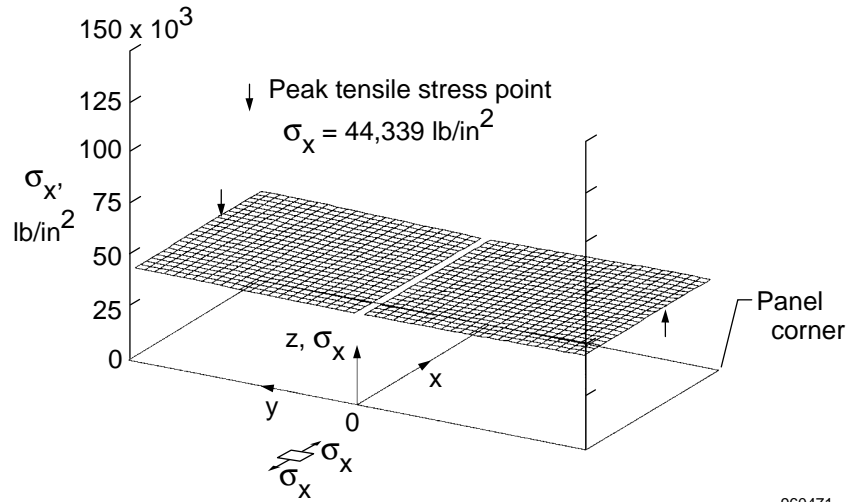

960454

Figure 14. Distribution of σ_y in the upper face sheet; 4S free-edge condition; flat temperature profile; $T_u = 900\ °\text{F}$, $T_l = 200\ °\text{F}$.
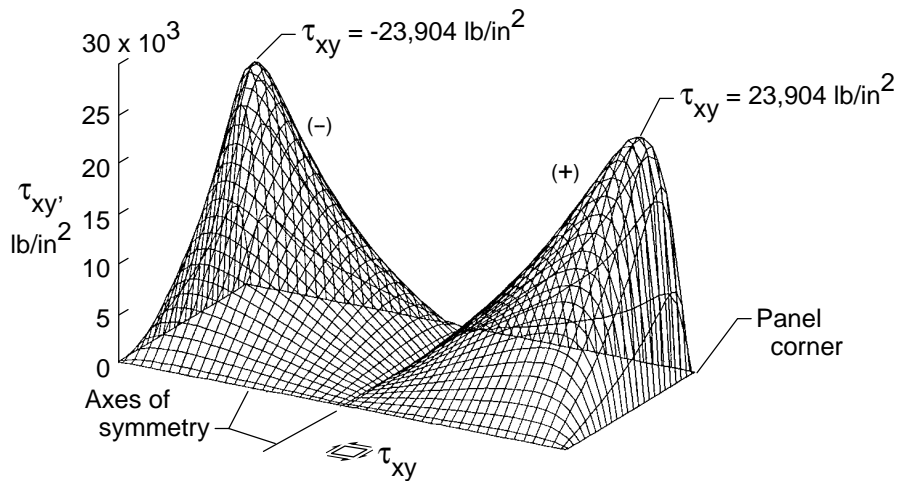
960455
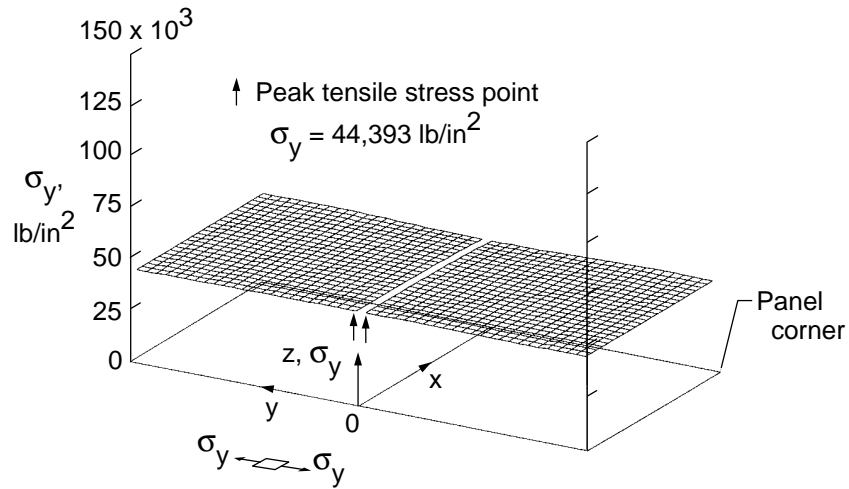
Figure 15. Distribution of τ_{xy} in the upper face sheet; 4S free-edge condition; flat temperature profile; $T_u = 900\ °\text{F}$, $T_l = 200\ °\text{F}$.
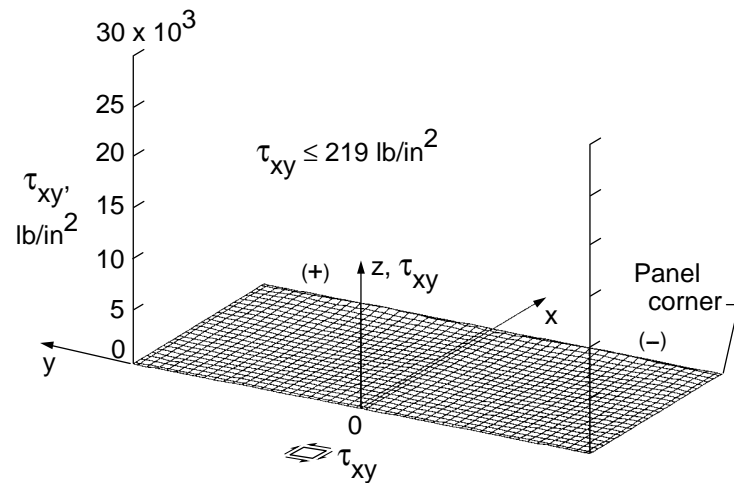
23
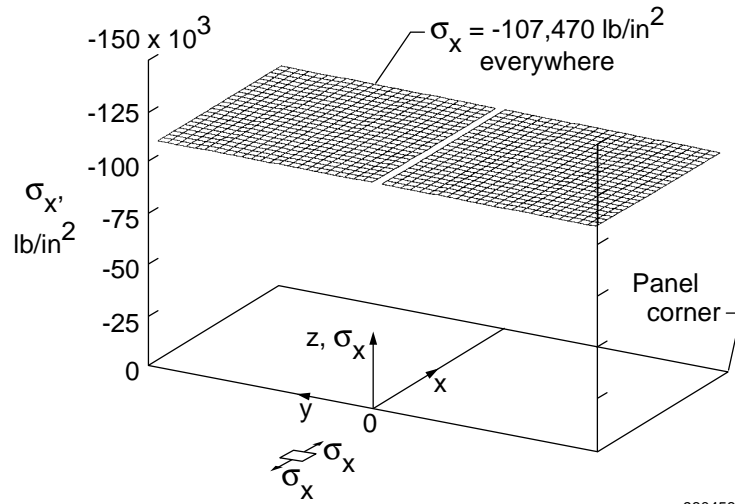
960456

Figure 16. Distribution of σ_x in the upper face sheet; 4C fixed-edge condition; flat temperature profile; $T_u = 900 \, °F$, $T_l = 200 \, °F$.
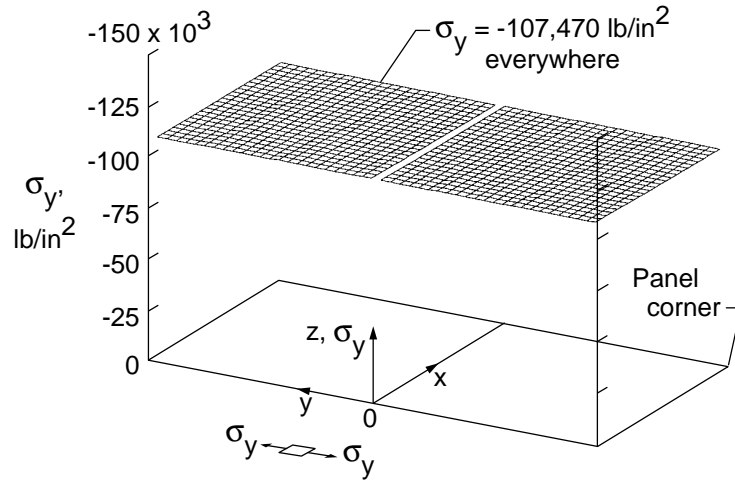
960457

Figure 17. Distribution of σ_y in the upper face sheet; 4C fixed-edge condition; flat temperature profile; $T_u = 900 \, °F$, $T_l = 200 \, °F$.
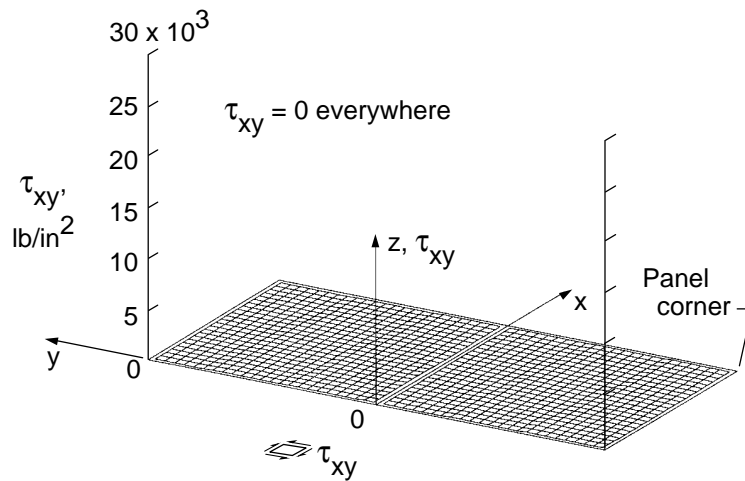
960458

Figure 18. Distribution of τ_{xy} in the upper face sheet; 4C fixed-edge condition; flat temperature profile; $T_u = 900 \, °F$, $T_l = 200 \, °F$.

24

960459
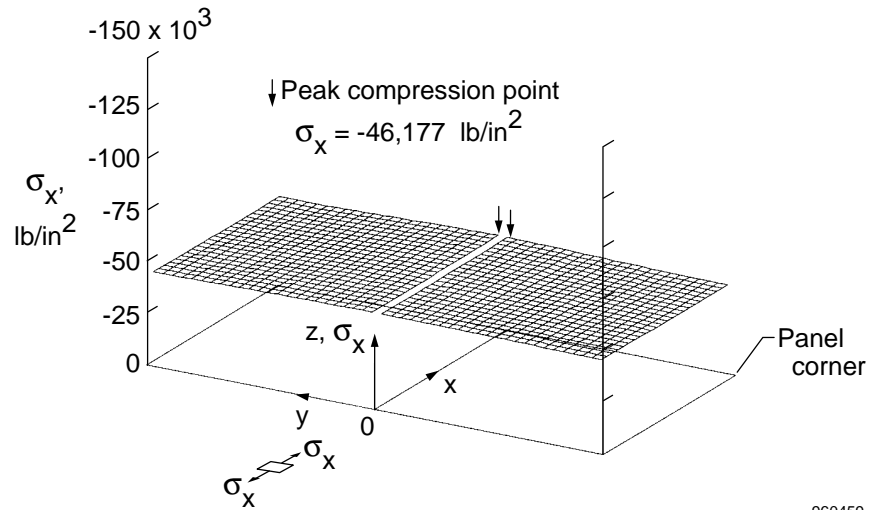
Figure 19. Distribution of σ_x in the upper face sheet; 4C free-edge condition; flat temperature profile; $T_u = 900\ °F$, $T_l = 200\ °F$.


960460
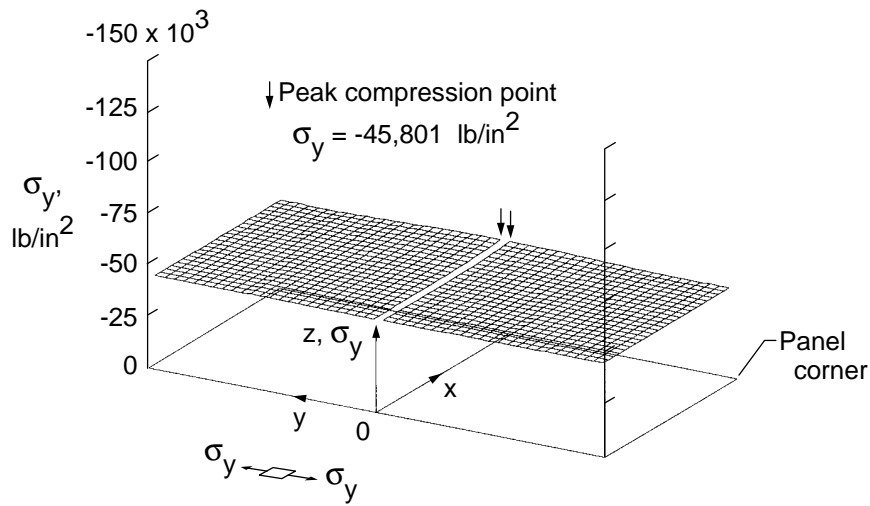
Figure 20. Distribution of σ_y in the upper face sheet; 4C free-edge condition; flat temperature profile; $T_u = 900\ °F$, $T_l = 200\ °F$.
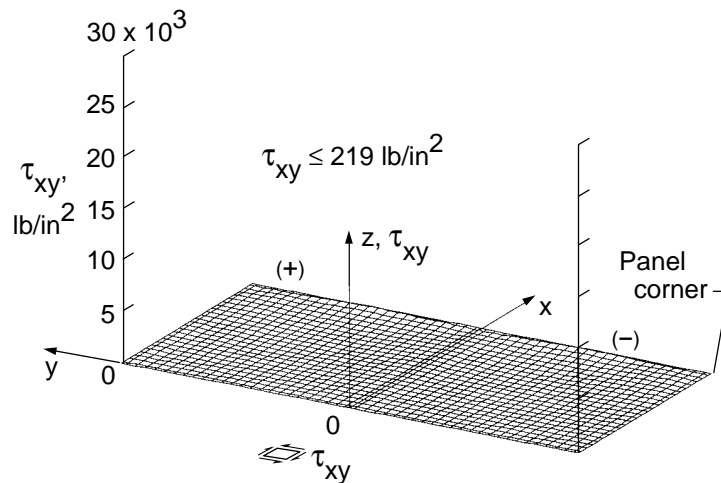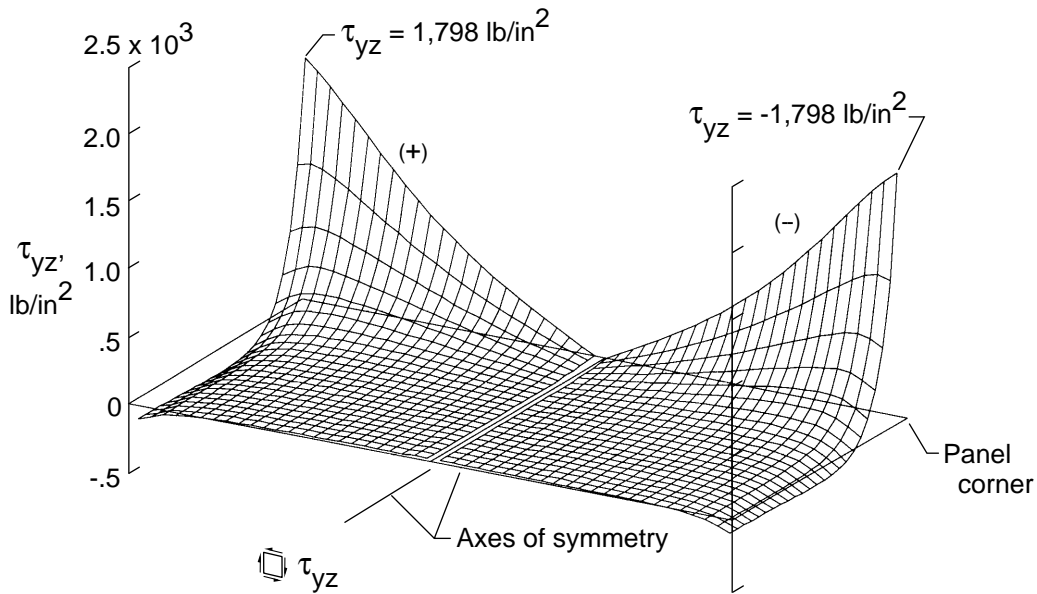

960461

Figure 21. Distribution of τ_{xy} in the upper face sheet; 4C free-edge condition; flat temperature profile; $T_u = 900\ °F$, $T_l = 200\ °F$.

25

Normal and Shear Stress Distributions in Lower Face Sheet—Flat Temperature Profile
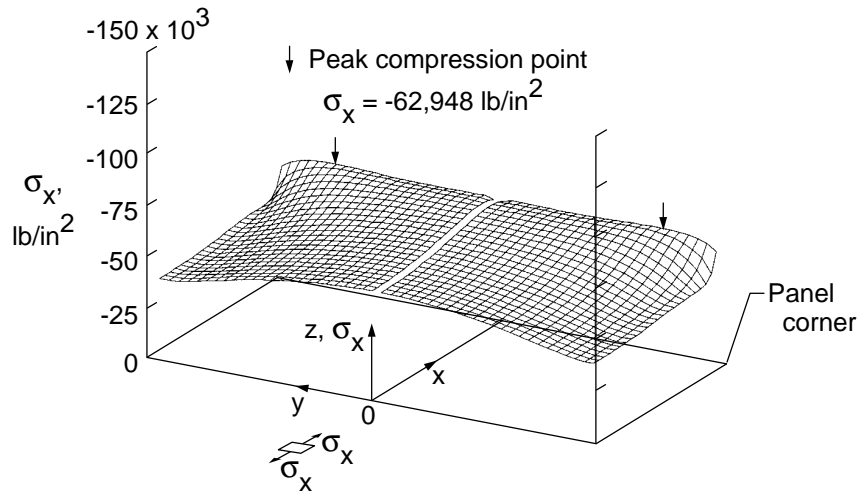
Figure 22. Distribution of σ_x in the lower face sheet; 4S fixed-edge condition; flat temperature profile; $T_u = 900$ °F, $T_l = 200$ °F.
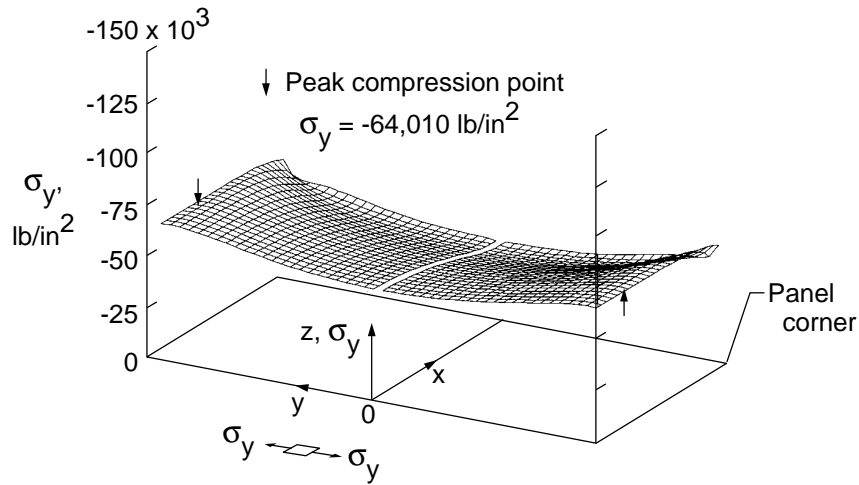
Figure 23. Distribution of σ_y in the lower face sheet; 4S fixed-edge condition; flat temperature profile; $T_u = 900$ °F, $T_l = 200$ °F.
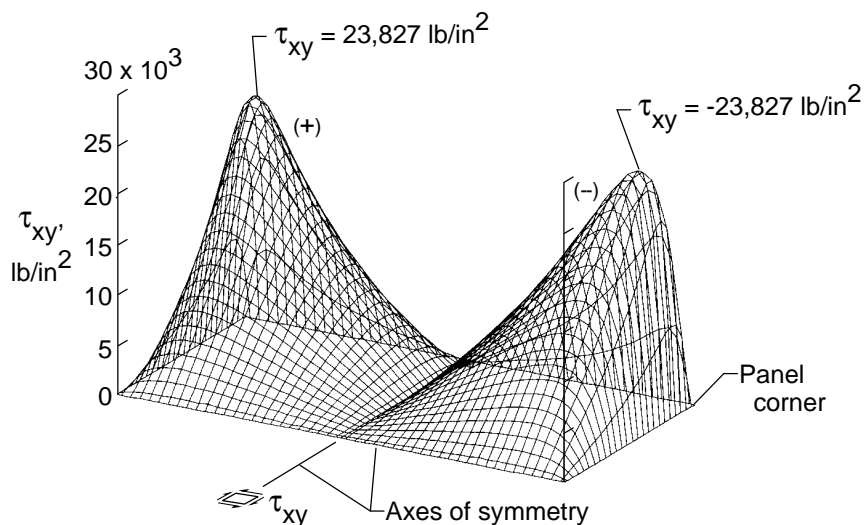
Figure 24. Distribution of τ_{xy} in the lower face sheet; 4S fixed-edge condition; flat temperature profile; $T_u = 900$ °F, $T_l = 200$ °F.

27

960465
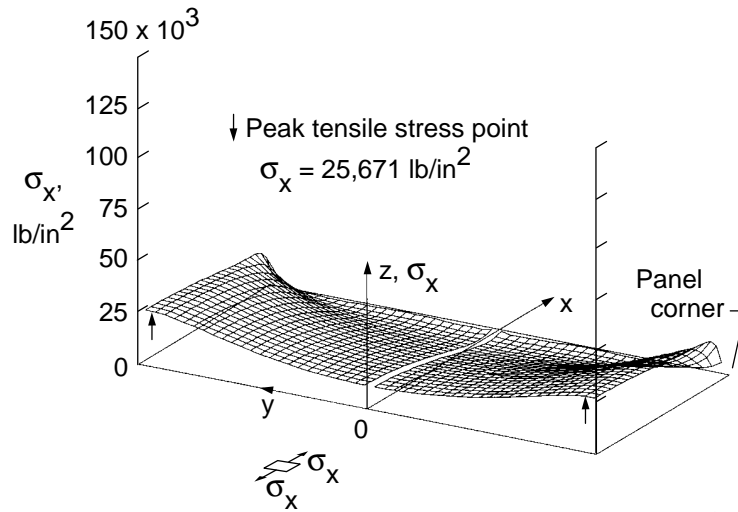
Figure 25. Distribution of σ_x in the lower face sheet; 4S free-edge condition; flat temperature profile; $T_u = 900\ °F$, $T_l = 200\ °F$.

960466
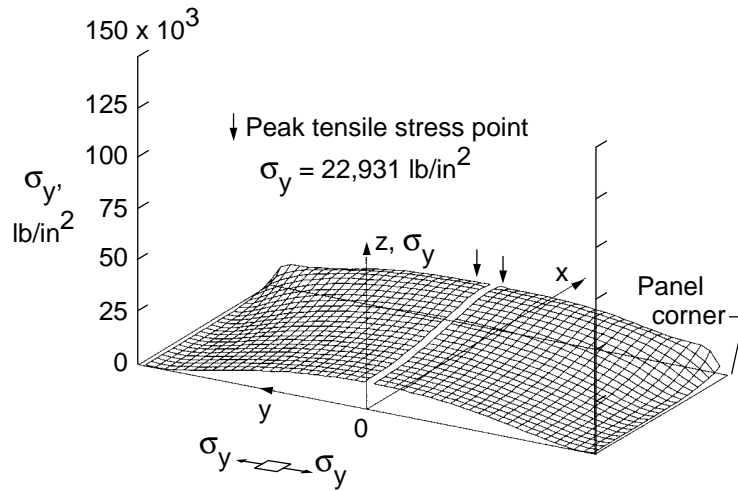
Figure 26. Distribution of σ_y in the lower face sheet; 4S free-edge condition; flat temperature profile; $T_u = 900\ °F$, $T_l = 200\ °F$.

960467
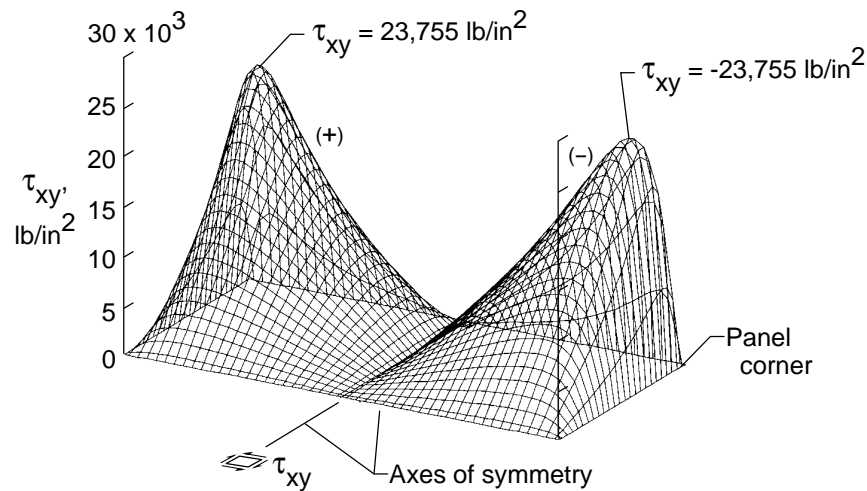
Figure 27. Distribution of τ_{xy} in the lower face sheet; 4S free-edge condition; flat temperature profile; $T_u = 900\ °F$, $T_l = 200\ °F$.

28

960468
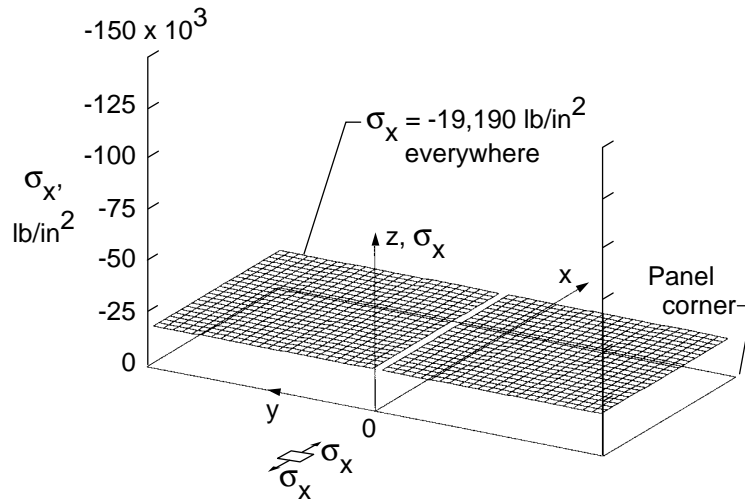
Figure 28. Distribution of σ_x in the lower face sheet; 4C fixed-edge condition; flat temperature profile; $T_u = 900\ °F$, $T_l = 200\ °F$.

960469

Figure 29. Distribution of σ_y in the lower face sheet; 4C fixed-edge condition; flat temperature profile; $T_u = 900\ °F$, $T_l = 200\ °F$.


960470

Figure 30. Distribution of τ_{xy} in the lower face sheet; 4C fixed-edge condition; flat temperature profile; $T_u = 900\ °F$, $T_l = 200\ °F$.

29

Figure 31. Distribution of σ_x in the lower face sheet; 4C free-edge condition; flat temperature profile; $T_u = 900\ {}^\circ\text{F}$, $T_l = 200\ {}^\circ\text{F}$.

Figure 32. Distribution of σ_y in the lower face sheet; 4C free-edge condition; flat temperature profile; $T_u = 900\ {}^\circ\text{F}$, $T_l = 200\ {}^\circ\text{F}$.

Figure 33. Distribution of τ_{xy} in the lower face sheet; 4C free-edge condition; flat temperature profile; $T_u = 900\ {}^\circ\text{F}$, $T_l = 200\ {}^\circ\text{F}$.

30
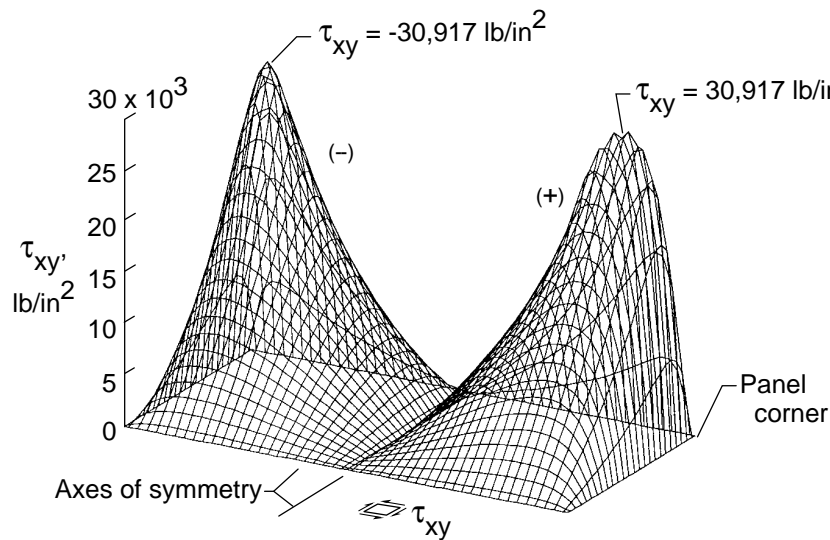
Transverse Sheer Stress Distributions in Sandwich Core—Flat Temperature Profile
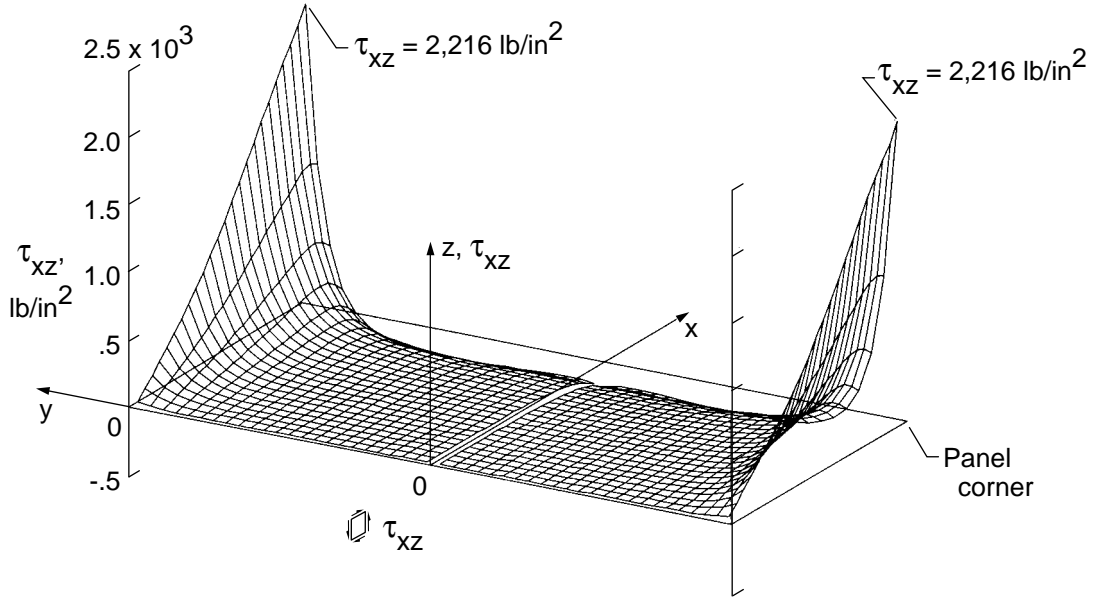
Figure 34. Distribution of transverse shear stress τ_{xz} in sandwich core; 4S fixed- or 4S free-edge condition; flat temperature profile; $T_u = 900\ °F$, $T_l = 200\ °F$.

Figure 35. Distribution of transverse shear stress τ_{yz} in sandwich core; 4S fixed- or 4S free-edge condition; flat temperature profile; $T_u = 900\ °F$, $T_l = 200\ °F$.
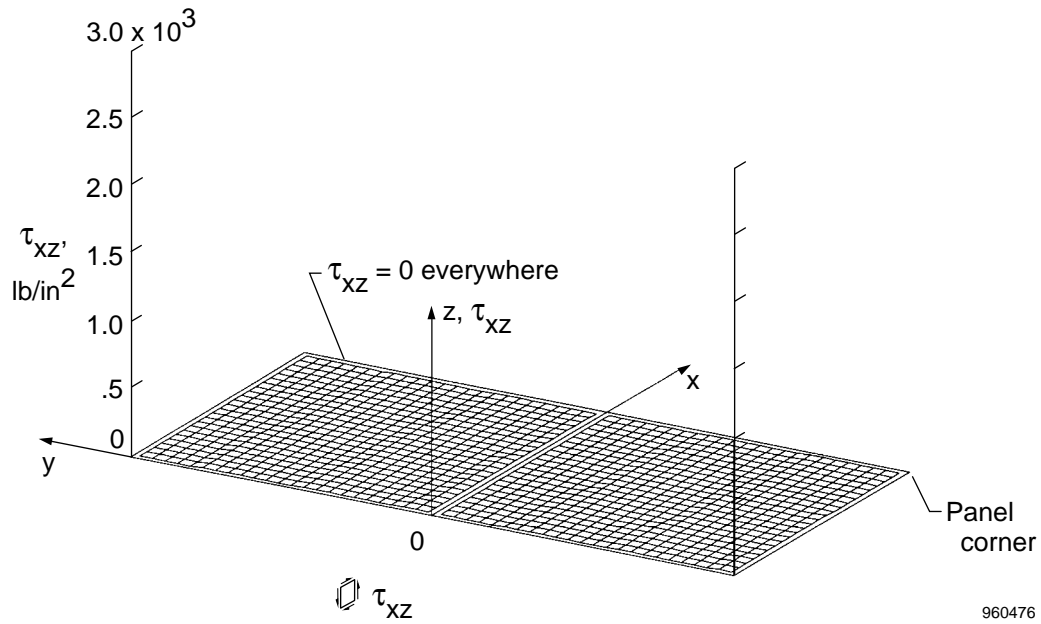
Figure 36. Distribution of transverse shear stress τ_{xz} in sandwich core; 4C fixed- or 4C free-edge condition; flat temperature profile; $T_u = 900$ °F, $T_l = 200$ °F.
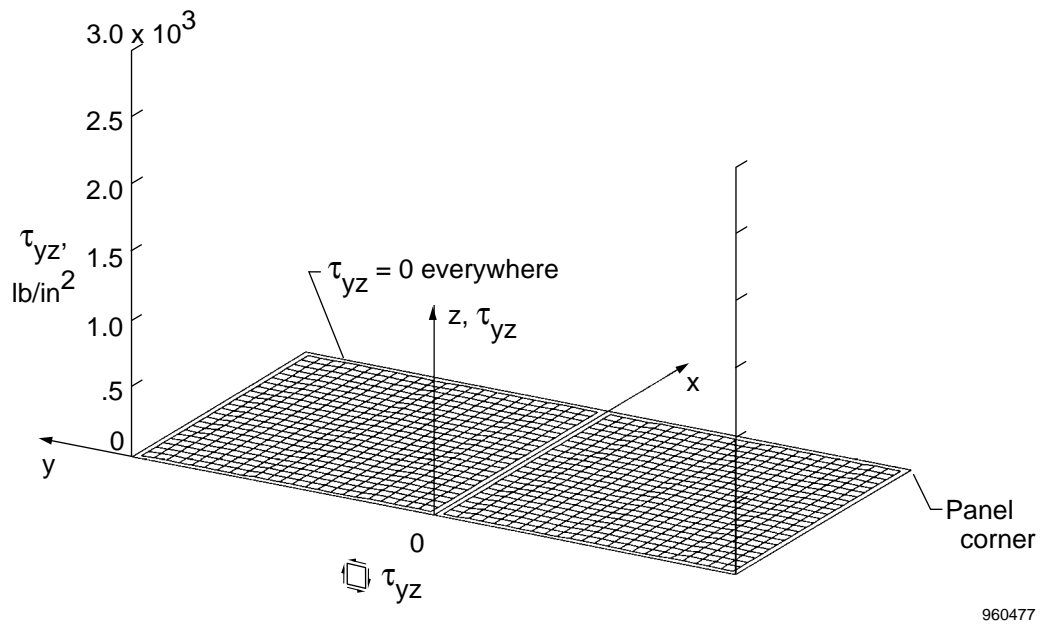
Figure 37. Distribution of transverse shear stress τ_{yz} in sandwich core; 4C fixed- or 4C free-edge condition; flat temperature profile; $T_u = 900$ °F, $T_l = 200$ °F.

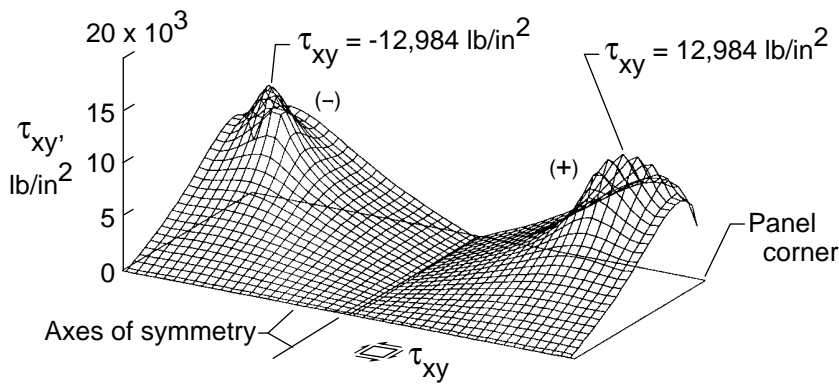**Normal and Shear Stress Distributions in Upper Face Sheet—Dome Temperature Profile**
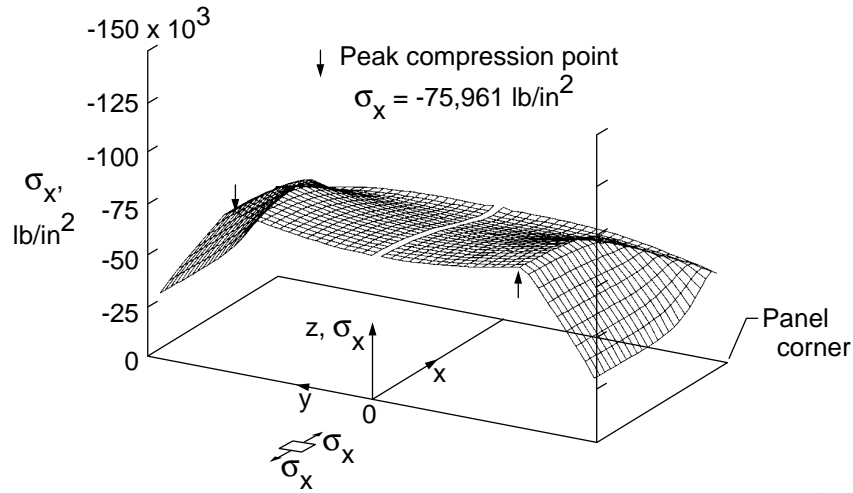
Figure 38. Distribution of σ_x in the upper face sheet; 4S fixed-edge condition; dome temperature profile; $T_u = 900\ °\text{F}$, $T_l = 200\ °\text{F}$.
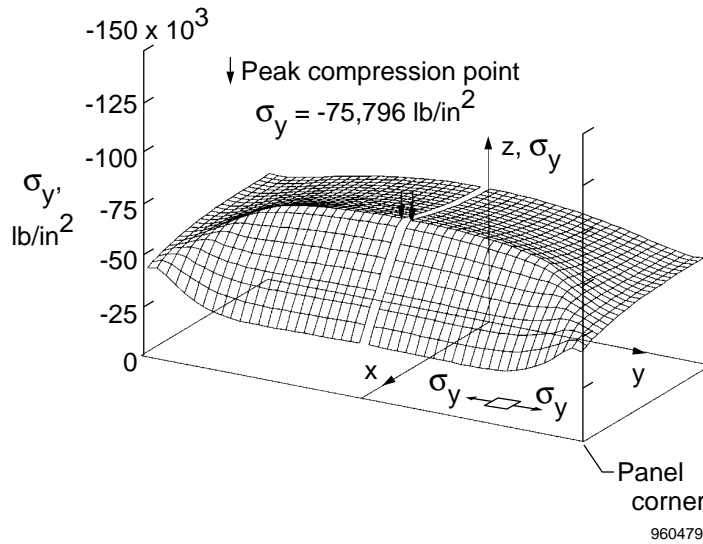
Figure 39. Distribution of σ_y in the upper face sheet; 4S fixed-edge condition; dome temperature profile; $T_u = 900\ °\text{F}$, $T_l = 200\ °\text{F}$.
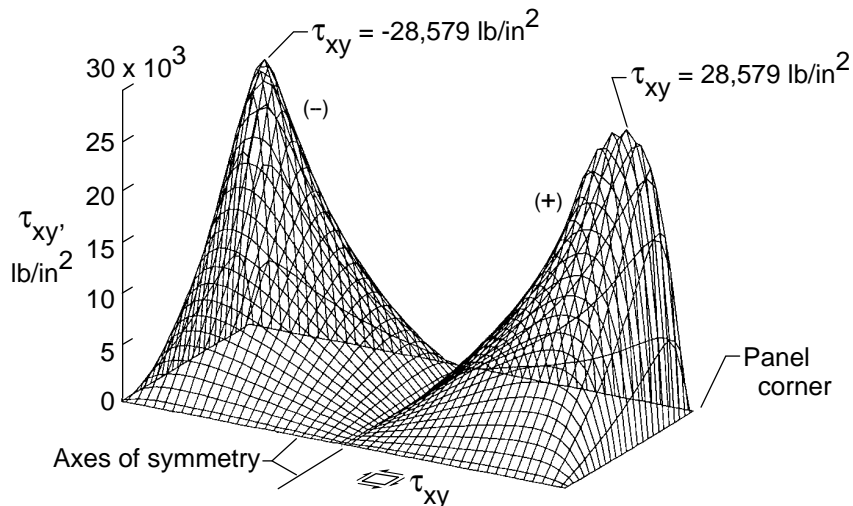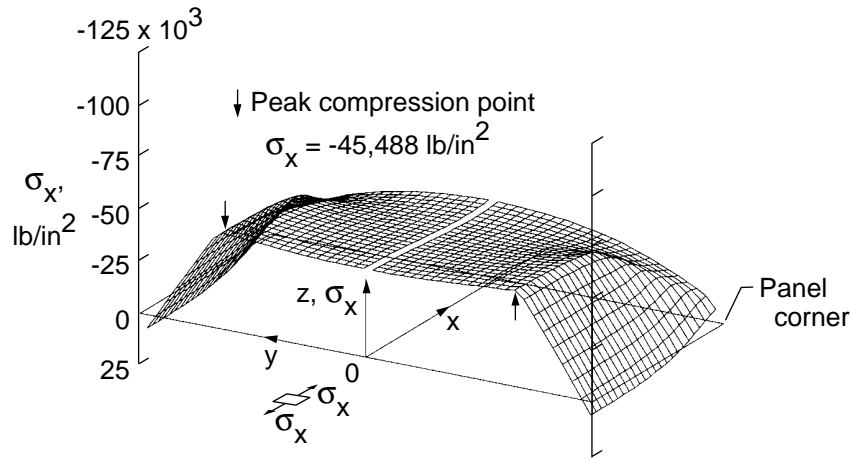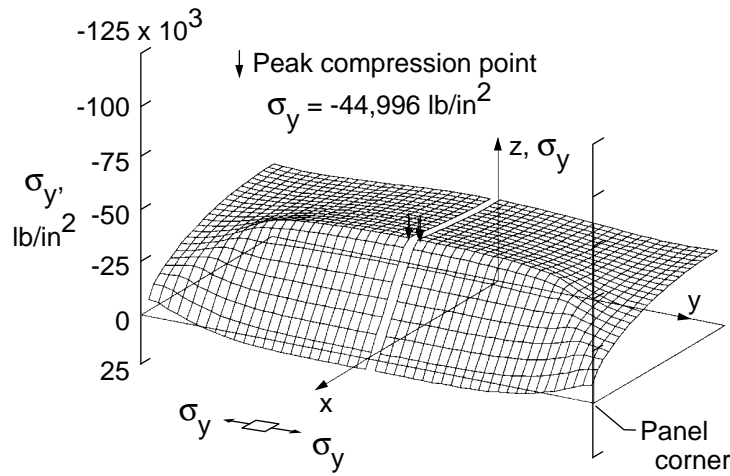

Figure 40. Distribution of τ_{xy} in the upper face sheet; 4S fixed-edge condition; dome temperature profile; $T_u = 900\ °\text{F}$, $T_l = 200\ °\text{F}$.

35

Figure 41

-100×10^3

↓ Peak compression point

$\sigma_x = -26{,}140 \text{ lb/in}^2$

-75

-50

z, σ_x

σ_x, lb/in^2

-25

x

Panel corner

0

y

25

0

50

σ_x σ_x

σ_x
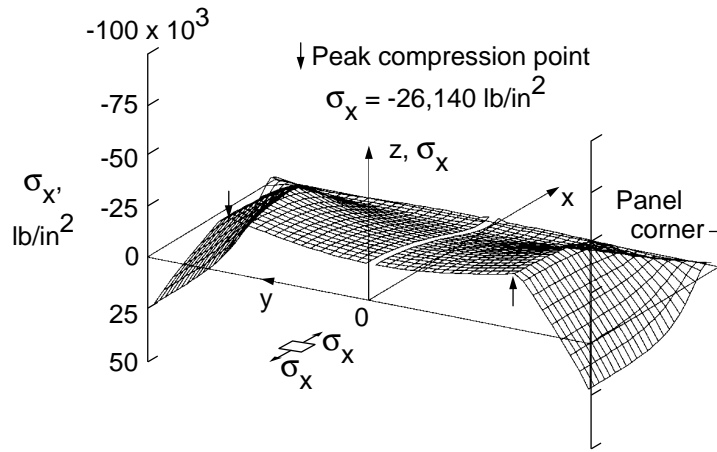
960481

Figure 41. Distribution of σ_x in the upper face sheet; 4S free-edge condition; dome temperature profile; $T_u = 900\ °\text{F}$, $T_l = 200\ °\text{F}$.

Figure 42

-100×10^3

↓ Peak compression point

$\sigma_y = -25{,}576 \text{ lb/in}^2$

-75

-50

z, σ_y

σ_y, lb/in^2

-25

0

y

25

x

50

Panel corner

σ_y σ_y
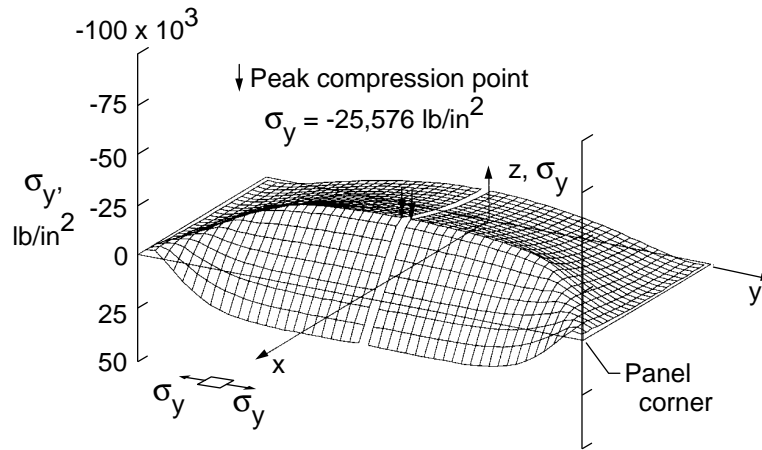
960482

Figure 42. Distribution of σ_y in the upper face sheet; 4S free-edge condition; dome temperature profile; $T_u = 900\ °\text{F}$, $T_l = 200\ °\text{F}$.

Figure 43

$\tau_{xy} = -30{,}917 \text{ lb/in}^2$

30×10^3

$\tau_{xy} = 30{,}917 \text{ lb/in}^2$

25

$(-)$

$(+)$

20

τ_{xy}, lb/in^2

15

10

5

Panel corner

0

Axes of symmetry

τ_{xy}

960483

Figure 43. Distribution of τ_{xy} in the upper face sheet; 4S free-edge condition; dome temperature profile; $T_u = 900\ °\text{F}$, $T_l = 200\ °\text{F}$.

36

-150 x 10^3 ↓ Peak compression point

σ_x = -96,192 lb/in^2

σ_x, lb/in^2

-125

-100

-75

-50

-25

0

z, σ_x
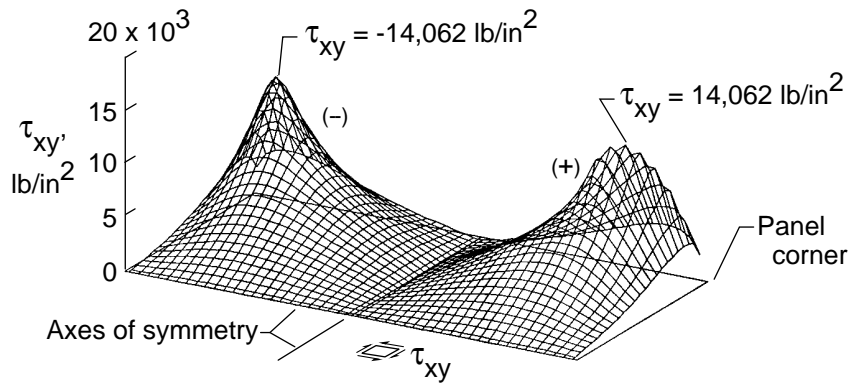
x

y

0

σ_x

σ_x

Panel corner
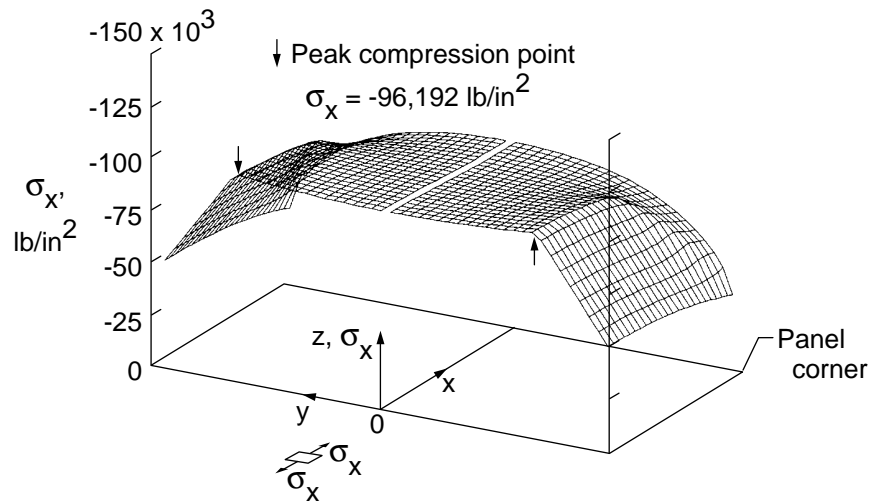
960484

Figure 44. Distribution of σ_x in the upper face sheet; 4C fixed-edge condition; dome temperature profile; $T_u = 900$ °F, $T_l = 200$ °F.

-150 x 10^3 ↓ Peak compression point

σ_y = -96,087 lb/in^2

z, σ_y

σ_y, lb/in^2

-125

-100

-75

-50

-25

0

σ_y

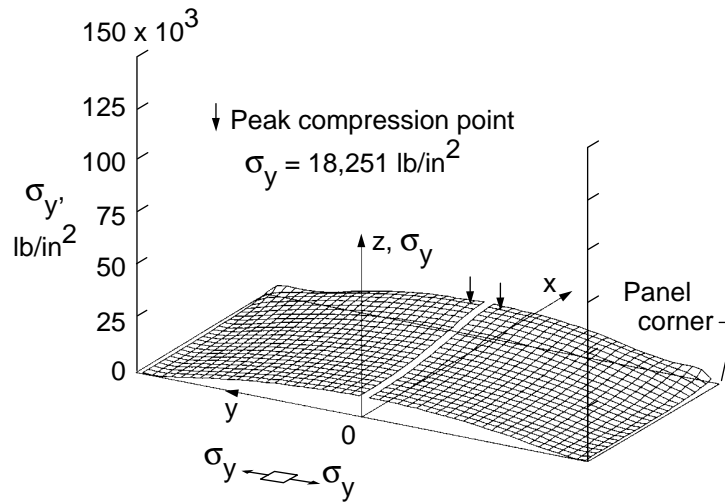σ_y

x

y

Panel corner
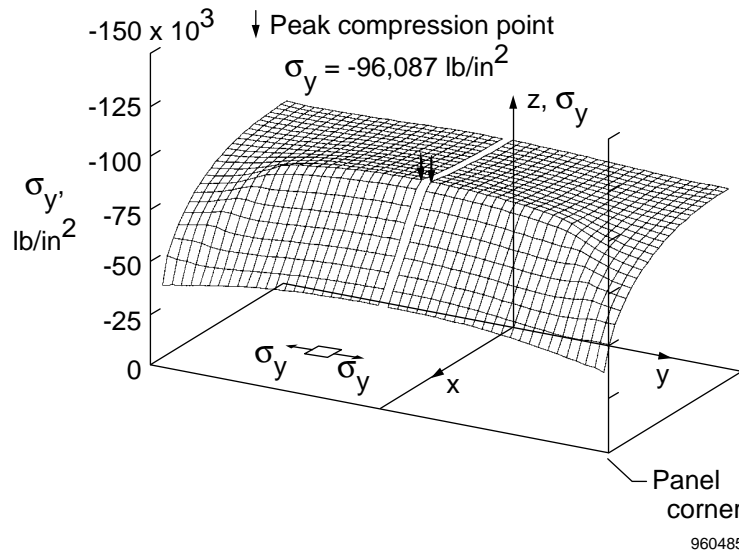
960485

Figure 45. Distribution of σ_y in the upper face sheet; 4C fixed-edge condition; dome temperature profile; $T_u = 900$ °F, $T_l = 200$ °F.

20 x 10^3 τ_{xy} = -12,984 lb/in^2 τ_{xy} = 12,984 lb/in^2

τ_{xy}, lb/in^2

15

(−)

10

(+)

5

0

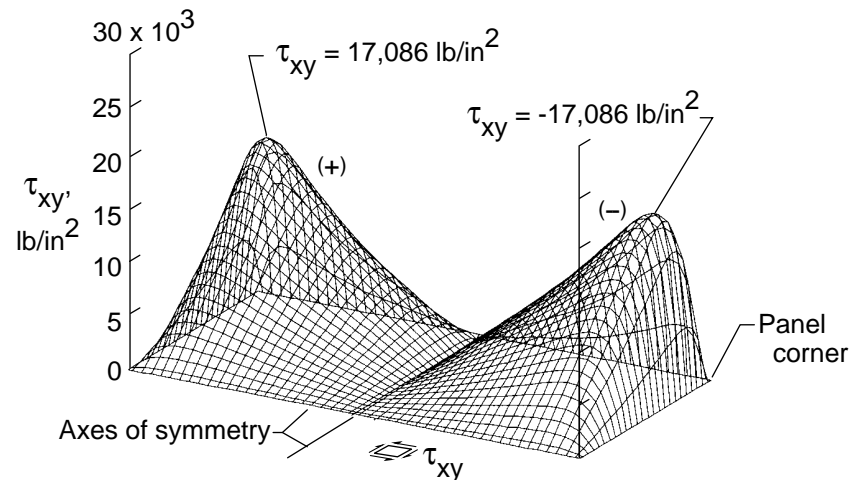Panel corner

Axes of symmetry

τ_{xy}

960486

Figure 46. Distribution of τ_{xy} in the upper face sheet; 4C fixed-edge condition; dome temperature profile; $T_u = 900$ °F, $T_l = 200$ °F.

37

960487

Figure 47. Distribution of σ_x in the upper face sheet; 4C free-edge condition; dome temperature profile; $T_u = 900\ °F$, $T_l = 200\ °F$.
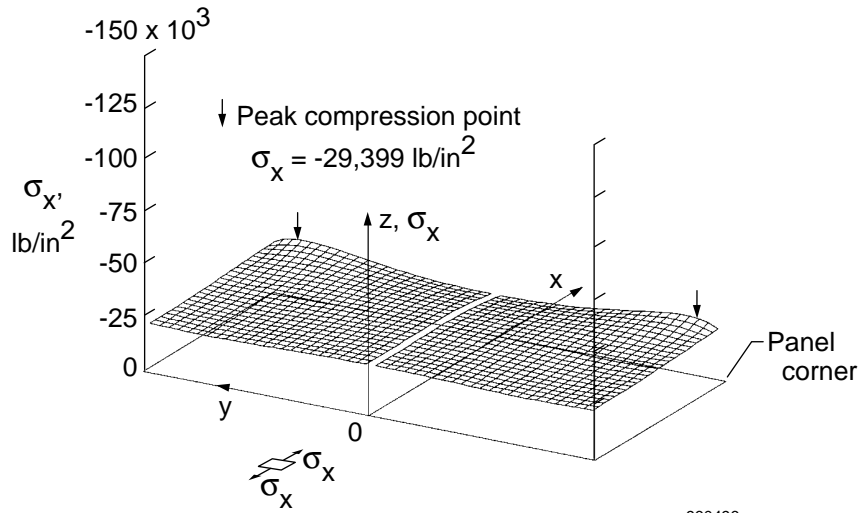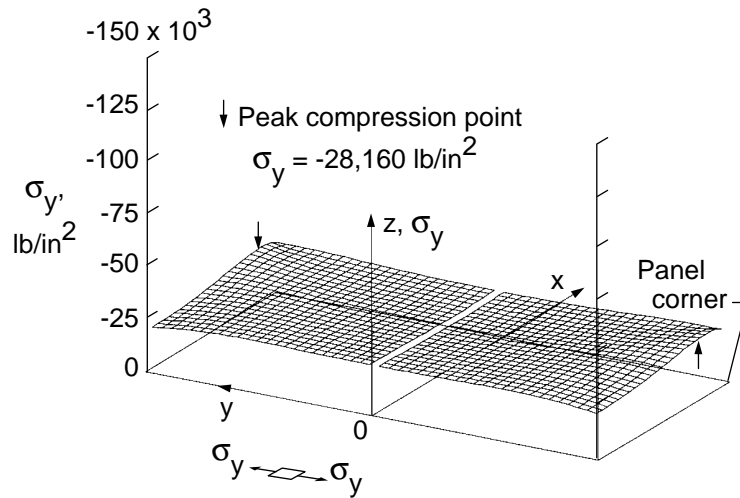

960488

Figure 48. Distribution of σ_y in the upper face sheet; 4C free-edge condition; dome temperature profile; $T_u = 900\ °F$, $T_l = 200\ °F$.

960489

Figure 49. Distribution of τ_{xy} in the upper face sheet; 4C free-edge condition; dome temperature profile; $T_u = 900\ °°F$, $T_l = 200\ °F$.

38

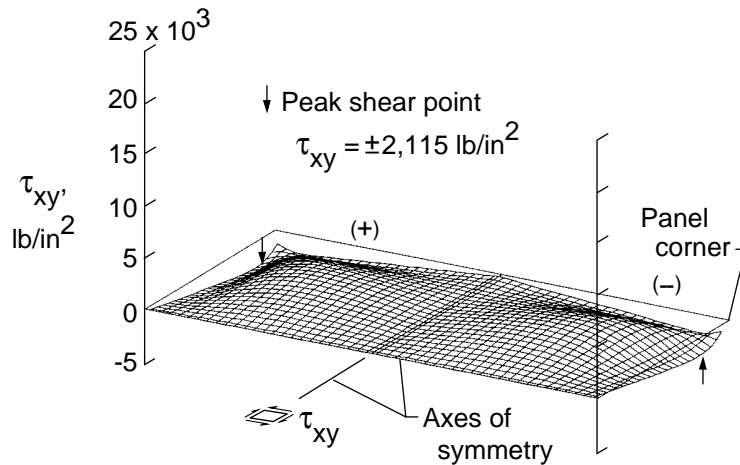**Normal and Shear Stress Distributions in Lower Face Sheet—Dome Temperature Profile**
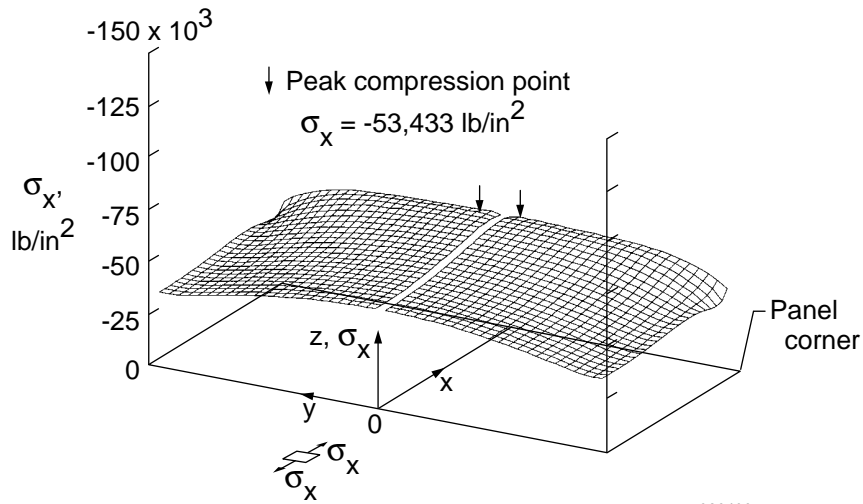
960490

Figure 50. Distribution of σ_x in the lower face sheet; 4S fixed-edge condition; dome temperature profile; $T_u = 900\ °F$, $T_l = 200\ °F$.
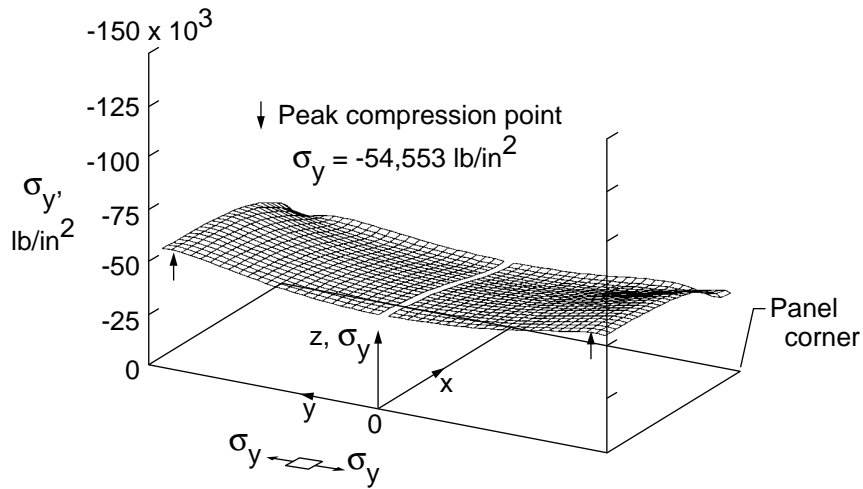
960491

Figure 51. Distribution of σ_y in the lower face sheet; 4S fixed-edge condition; dome temperature profile; $T_u = 900\ °F$, $T_l = 200\ °F$.
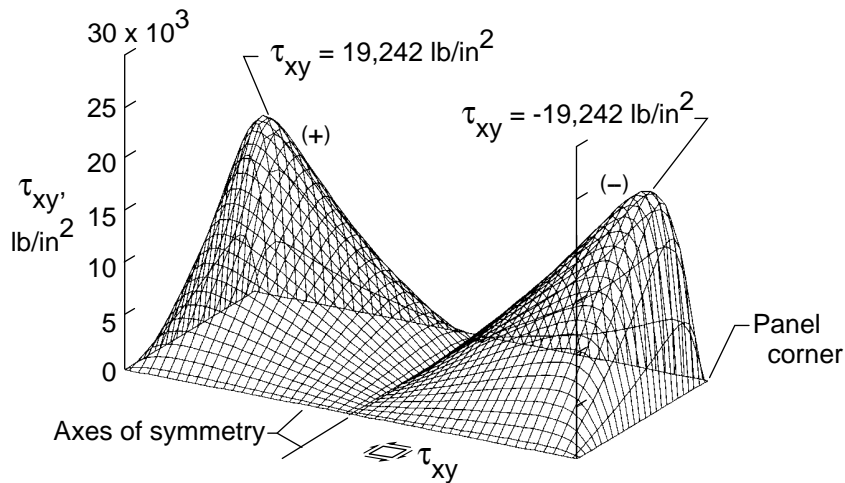
960492

Figure 52. Distribution of τ_{xy} in the lower face sheet; 4S fixed-edge condition; dome temperature profile; $T_u = 900\ °F$, $T_l = 200\ °F$.

40

960493
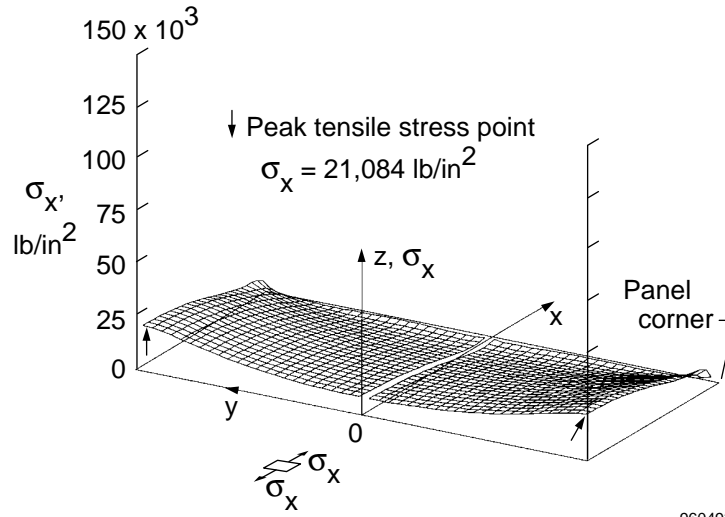
Figure 53. Distribution of σ_x in the lower face sheet; 4S free-edge condition; dome temperature profile; $T_u = 900\ °\text{F}$, $T_l = 200\ °\text{F}$.
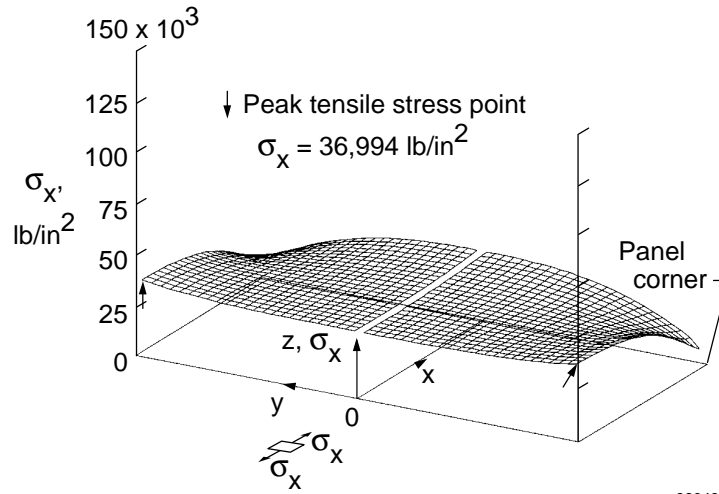

960494

Figure 54. Distribution of σ_y in the lower face sheet; 4S free-edge condition; dome temperature profile; $T_u = 900\ °\text{F}$, $T_l = 200\ °\text{F}$.

960495

Figure 55. Distribution of τ_{xy} in the lower face sheet; 4S free-edge condition; dome temperature profile; $T_u = 900\ °\text{F}$, $T_l = 200\ °\text{F}$.

41

Figure 56. Distribution of σ_x in the lower face sheet; 4C fixed-edge condition; dome temperature profile; $T_u = 900\ °F$, $T_l = 200\ °F$.
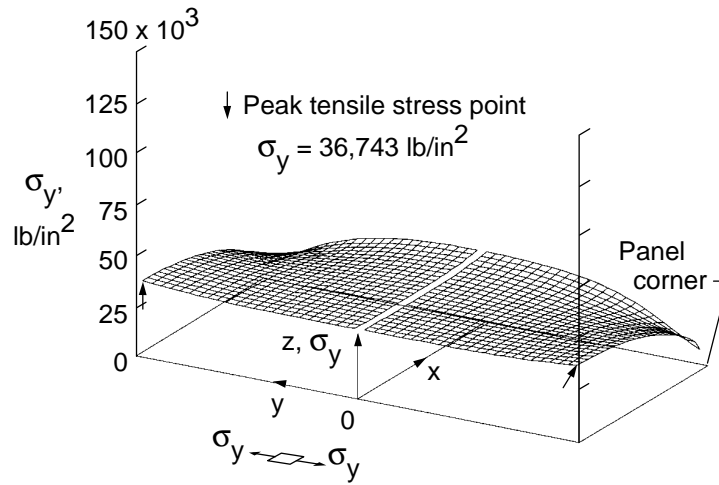

Figure 57. Distribution of σ_y in the lower face sheet; 4C fixed-edge condition; dome temperature profile; $T_u = 900\ °F$, $T_l = 200\ °F$.
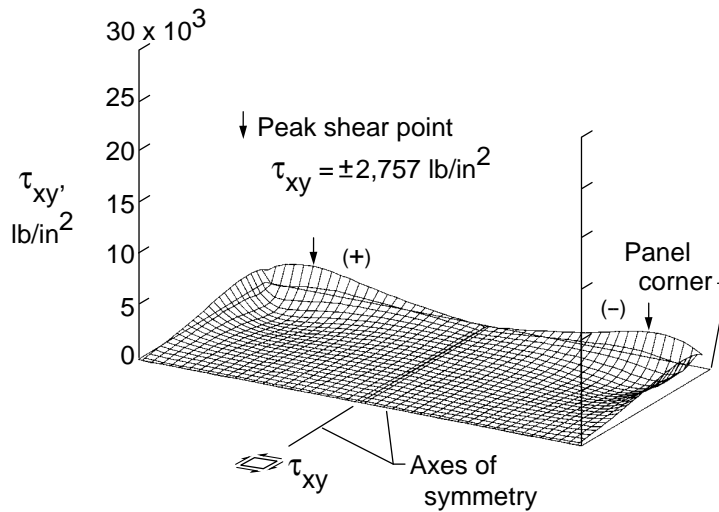

Figure 58. Distribution of τ_{xy} in the lower face sheet; 4C fixed-edge condition; dome temperature profile; $T_u = 900\ °F$, $T_l = 200\ °F$.

42

Figure 59. Distribution of σ_x in the lower face sheet; 4C free-edge condition; dome temperature profile; $T_u = 900\ °\text{F}$, $T_l = 200\ °\text{F}$.

Figure 60. Distribution of σ_y in the lower face sheet; 4C free-edge condition; dome temperature profile; $T_u = 900\ °\text{F}$, $T_l = 200\ °\text{F}$.

Figure 61. Distribution of τ_{xy} in the lower face sheet; 4C free-edge condition; dome temperature profile; $T_u = 900\ °\text{F}$, $T_l = 200\ °\text{F}$.

43

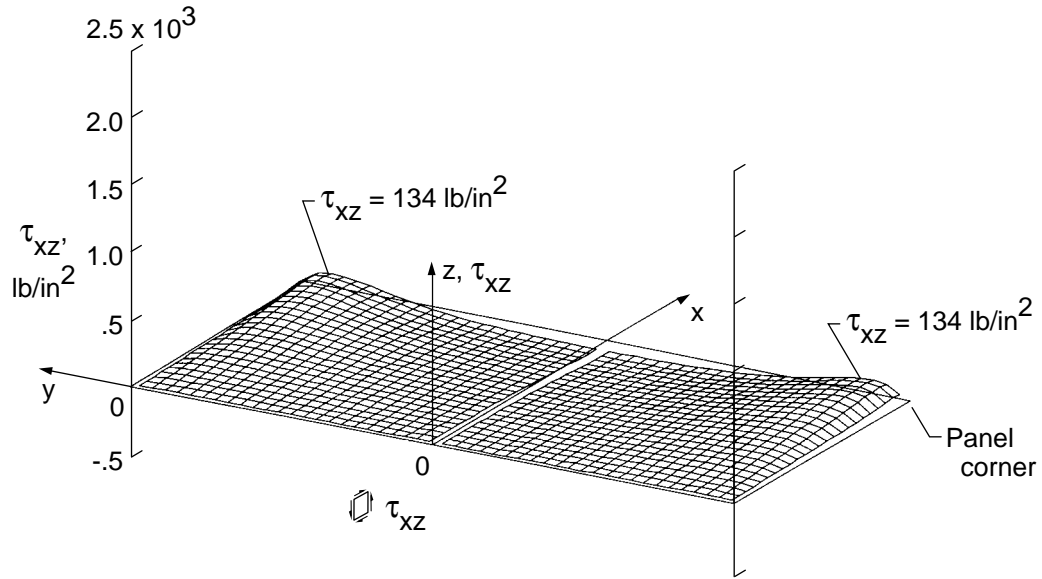**Transverse Shear Stress Distributions in Sandwich Core—Dome Temperature Profile**
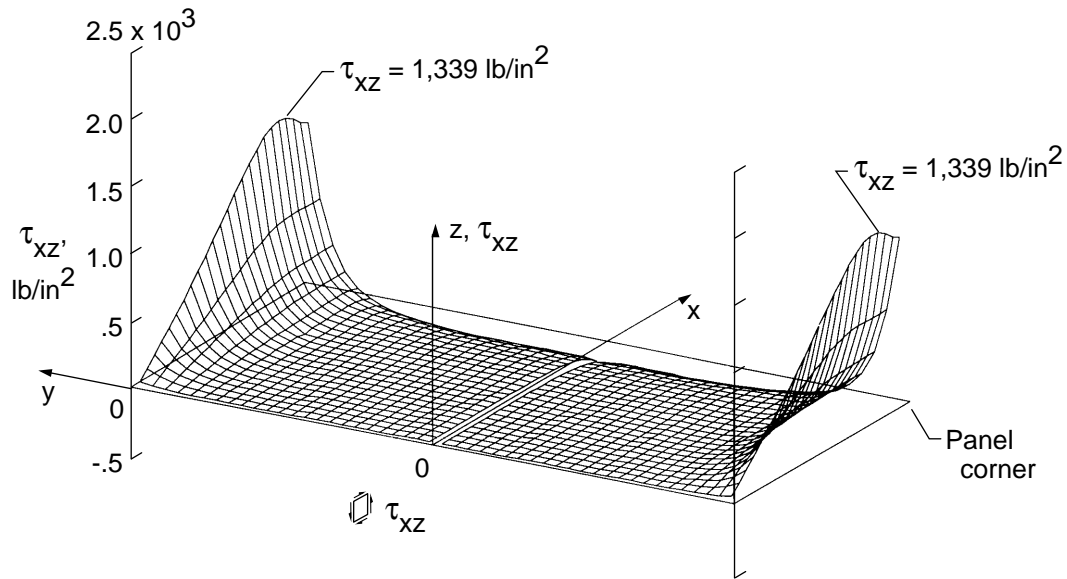
Figure 62. Distribution of transverse shear stress τ_{xz} in sandwich core; 4S fixed- or 4S free-edge condition; dome temperature profile; $T_u = 900$ °F, $T_l = 200$ °F.
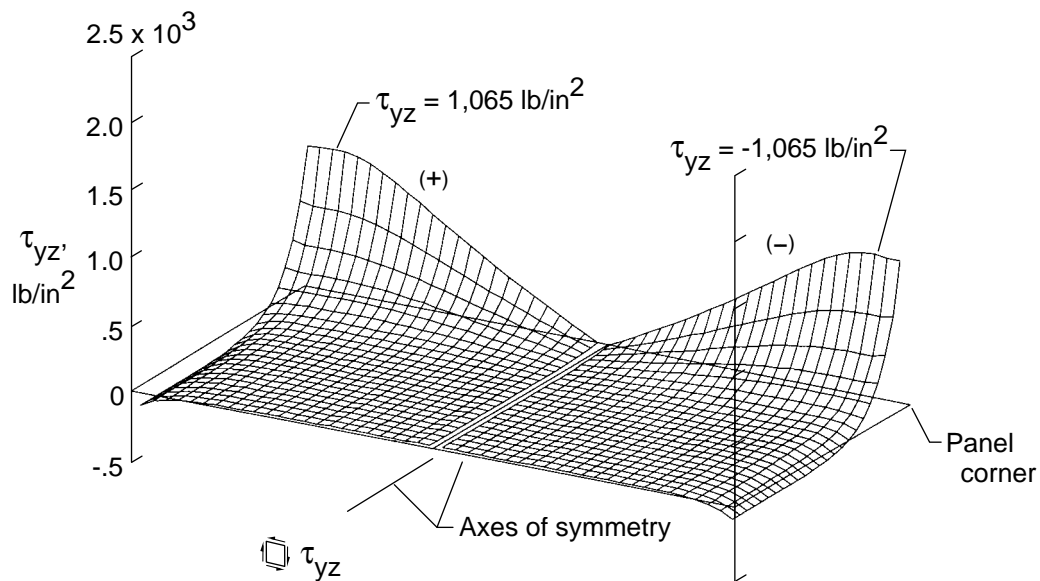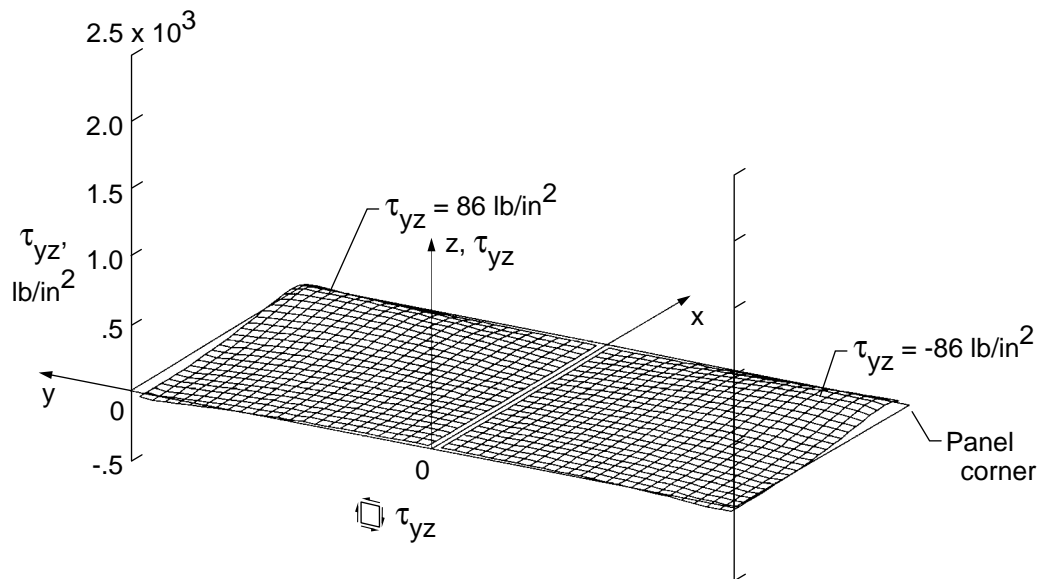

Figure 63. Distribution of transverse shear stress τ_{yz} in sandwich core; 4S fixed- or 4S free-edge condition; dome temperature profile; $T_u = 900$ °F, $T_l = 200$ °F.
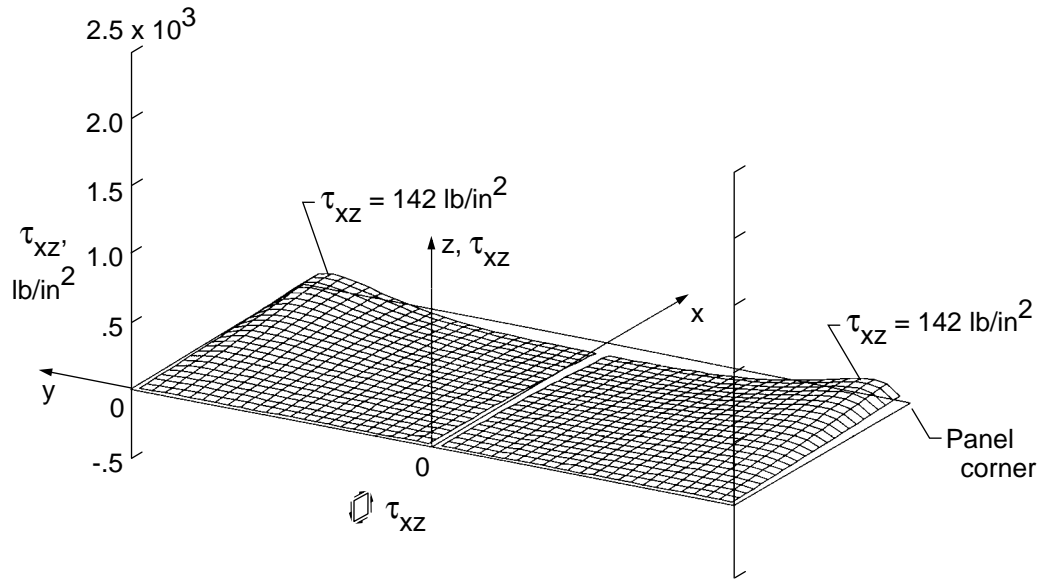
45

Figure 64. Distribution of transverse shear stress τ_{xz} in sandwich core; 4C fixed-edge condition; dome temperature profile; $T_u = 900\ °F$, $T_l = 200\ °F$.
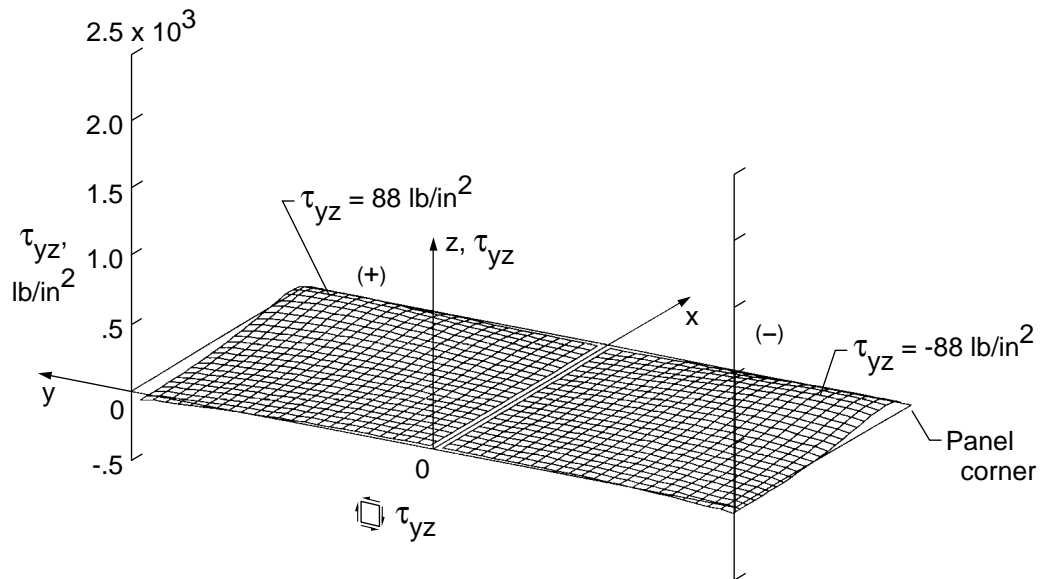

Figure 65. Distribution of transverse shear stress τ_{yz} in sandwich core; 4C fixed-edge condition; dome temperature profile; $T_u = 900\ °F$, $T_l = 200\ °F$.

960506

Figure 66. Distribution of transverse shear stress τ_{xz} in sandwich core; 4C free-edge condition; dome temperature profile; $T_u = 900\ °F$, $T_l = 200\ °F$.

960507

Figure 67. Distribution of transverse shear stress τ_{yz} in sandwich core; 4C free-edge condition; dome temperature profile; $T_u = 900\ °F$, $T_l = 200\ °F$.

47

REPORT DOCUMENTATION PAGE

1. AGENCY USE ONLY (Leave blank)	2. REPORT DATE April 1997	3. REPORT TYPE AND DATES COVERED Technical Memorandum

4. TITLE AND SUBTITLE

Thermostructural Behavior of a Hypersonic Aircraft Sandwich Panel Subjected to Heating on One Side

6. AUTHOR(S)

William L. Ko

5. FUNDING NUMBERS

WU 505-63-50-00-RS-00-000-01

7. PERFORMING ORGANIZATION NAME(S) AND ADDRESS(ES)

NASA Dryden Flight Research Center
P.O. Box 273
Edwards, California 93523-0273

8. PERFORMING ORGANIZATION REPORT NUMBER

H-2103

9. SPONSORING/MONOTORING AGENCY NAME(S) AND ADDRESS(ES)

National Aeronautics and Space Administration
Washington, DC 20546-0001

10. SPONSORING/MONITORING AGENCY REPORT NUMBER

NASA TM-4769

11. SUPPLEMENTARY NOTES

12a. DISTRIBUTION/AVAILABILITY STATEMENT

Unclassified—Unlimited
Subject Category 39

12b. DISTRIBUTION CODE

13. ABSTRACT (Maximum 200 words)

Thermostructural analysis was performed on a heated titanium honeycomb-core sandwich panel. The sandwich panel was supported at its four edges with spar-like substructures that acted as heat sinks, which are generally not considered in the classical analysis. One side of the panel was heated to high temperature to simulate aerodynamic heating during hypersonic flight. Two types of surface heating were considered: (1) flat-temperature profile, which ignores the effect of edge heat sinks, and (2) dome-shaped-temperature profile, which approximates the actual surface temperature distribution associated with the existence of edge heat sinks. The finite-element method was used to calculate the deformation field and thermal stress distributions in the face sheets and core of the sandwich panel. The detailed thermal stress distributions in the sandwich panel are presented, and critical stress regions are identified. The study shows how the magnitudes of those critical stresses and their locations change with different heating and edge conditions. This technical report presents comprehensive, three-dimensional graphical displays of thermal stress distributions in every part of a titanium honeycomb-core sandwich panel subjected to hypersonic heating on one side. The plots offer quick visualization of the structural response of the panel and are very useful for hot structures designers to identify the critical stress regions.

14. SUBJECT TERMS

Heat-sink effect, One-sided heating, Sandwich panels, Thermal deformations, Thermal stress analysis, Thermal stress distributions

15. NUMBER OF PAGES
52

16. PRICE CODE
A04

17. SECURITY CLASSIFICATION OF REPORT	18. SECURITY CLASSIFICATION OF THIS PAGE	19. SECURITY CLASSIFICATION OF ABSTRACT	20. LIMITATION OF ABSTRACT
Unclassified	Unclassified	Unclassified	Unlimited